J. Iron Steel Res. Int. (2021) 28:1483–1503
https://doi.org/10.1007/s42243-021-00700-4

REVIEW

Non-metallic inclusions in electroslag remelting: a review

Cheng-bin Shi[1] · Shi-jun Wang[1] · Jing Li[1] · Jung-wook Cho[2]

Received: 30 September 2021 / Revised: 5 November 2021 / Accepted: 6 November 2021 / Published online: 8 January 2022

Abstract
Non-metallic inclusion in electroslag remelting is a constant topic that has been studied for decades. Different results and conclusions are obtained on some of the subjects from these previous investigations. These differences originate in part from different experimental conditions, including original inclusion chemistries in consumable electrode, slag composition, oxygen level, liquid metal compositions, deoxidation schemes, and melting rates of electroslag remelting. The advances in the operating practices of inclusion control in electroslag remelting production are reviewed. Inclusion evolution during the electroslag remelting and related processing parameters are also reviewed and assessed. The role of the reoxidation of liquid steel during electroslag remelting on oxide inclusion composition is discussed. The generation of inclusions in remelted ingot is critically assessed. Perspective and remaining issues are noted.

Keywords Non-metallic inclusion · Electroslag remelting · Inclusion removal · Reoxidation

1 Introduction

The detriments of non-metallic inclusions (NMI) to the steel properties have been widely recognized, including surface quality [1], fatigue strength [2, 3], toughness and ductility [4, 5], impact strength [5], tensile properties [6], corrosion resistance [7, 8], initiation of fatigue cracking [9], and stress concentration cracking [5, 10]. Electroslag remelting (ESR) has been widely used to produce some varieties of high-quality steel and alloy, mainly because of its ability to drastically remove non-metallic inclusions and provide a superior solidification structure simultaneously [11–14]. With increasing demands for excellent properties of steel and alloy, more and more efforts have to be put forward to further improve steel cleanliness and precise control of non-metallic inclusions with respect to their chemical compositions, amount, size, morphology, and distribution during steelmaking and alloy manufacture process.

In comparison with other steelmaking technologies, electroslag remelting has absolute superiority to remove inclusions from liquid steel. In addition, unlike these steelmaking technologies, there are no exogenous inclusions in liquid steel from erosion of lining refractory. Although several studies indicate that 50% or more of the oxide inclusions in the remelted ingots are relics from the consumable steel electrode [15, 16], it is a general case that most of original inclusions (all original oxide for some types, sulfide, and nitride inclusions in some cases as discussed in Sect. 3.1) are removed during ESR, and there remain many small inclusions in the remelted ingots (even large inclusions occasionally in some cases) [17–21]. In this article, the inclusions in the consumable electrode are termed as the original inclusion. Generally, the inclusions are small in both small and large remelted ingots (mostly < 6 μm) [22–26]. It is the reason that the bearing steel with a larger amount of inclusions produced by ESR has a higher fatigue life in comparison with that with a lower oxygen content produced by other refining processing practices [27–29].

Electroslag remelting combines liquid metal refining and solidification structure control in one set. The inclusion evolution and the role of processing parameters of ESR on inclusions are different from those in other steelmaking

✉ Cheng-bin Shi
chengbin.shi@ustb.edu.cn

[1] Institute of Advanced Steel, State Key Laboratory of Advanced Metallurgy, University of Science and Technology Beijing (USTB), Beijing 100083, China

[2] Graduate Institute of Ferrous and Energy Materials Technology, Pohang University of Science and Technology (POSTECH), Pohang 790-784, Republic of Korea

processing. As the last processing step of liquid metal refining before solidification, the effects of ESR processing variables on inclusions have been the subject of many investigations over past decades. Most of these previous studies aim to maximize the removal of inclusions, prevent the generation of large inclusions, and target desired compositions of remaining inclusions. ESR is becoming increasingly more significant for high-quality steel production. Currently, the focus of the studies regarding ESR still lies on the inclusion control, besides lowering the oxygen content, suppressing the loss of alloying elements (such as Ti, Al, Si, and Mn in liquid metal [22, 30, 31]) and optimizing the solidification structure of as-cast ingot.

Improving cleanliness level of steel is still a challenge for the electroslag remelting. Regarding the cleanliness, the deoxidation and desulfurization as well as non-metallic inclusions in the ESR are its focus. Deoxidation and desulfurization in the ESR have been discussed in recent reviews [32, 33]. A good understanding of the inclusion evolution and removal in the ESR process as well as related processing parameters will be greatly helpful for inclusion control. In the present work, inclusion removal at different stages of ESR are evaluated first. Next, the evolution of different types of inclusions is reviewed and critically assessed. The crucial factors affecting inclusion characteristics in ESR are presented and discussed. This paper concludes with a general remark and perspective for future work.

2 Sites of inclusions removal during ESR

In the early years of booming ESR (1960s–1980s), the studies on non-metallic inclusions have been focused on revealing the removal sites (electrode tip, molten slag pool, and liquid metal pool) of oxide inclusions during the ESR process. The early researchers claimed that the inclusions removal during ESR process is the result of inclusion floating up in liquid metal pool and then absorbed by molten slag [34, 35]. However, this viewpoint ignores the reactions of inclusion–steel–slag system in the ESR process. The results from examining the steel samples taken from the electrode, metal droplets at electrode tip, dropping metal droplets, liquid metal pool and remelted ingot in Ref [36]. demonstrate that almost all original oxide inclusions in the steel electrode are removed before they enter into the liquid metal pool during the ESR process and most of the original oxide inclusions are removed at the electrode tip during liquid metal films formation and their collection into metal droplets. Li et al. [37, 38] proposed that the removal of inclusions occurred mainly at the electrode tip during liquid metal droplets formation in ESR of bearing steel, most of the original inclusions in electrode were removed at the electrode tip, and inclusion removal in liquid metal pool plays a minor role. Evseyev and Filippov [39] also demonstrated that the majority of the oxide inclusions in electrode was removed at the electrode tip during ESR.

The mechanism of inclusion removal proposed by Kay and Pomfret [40] is that oxide inclusions dissolve in the liquid metal at the electrode tip and that oxygen and deoxidant are transferred to slag by slag–metal reactions taking place at the tip interface, metal droplet–slag interface, and slag–metal pool interface. In contrast, Mitchell [41] claimed that the physical dissolution of inclusions is a minor part of overall inclusion removal. The present authors claim that the contribution degree of the dissolution of inclusions to overall inclusion removal differs according to the types of the inclusions, and examples of sulfide inclusion removal through its full dissolution will be discussed in Sect. 3.2. Removal of inclusions by flotation from bulk liquid in the liquid metal pool during ESR is always considered unlikely [40–42].

It is the adhesion and absorption of oxide inclusions by molten slag, because the thickness of liquid metal film is very small at the electrode tip that contributes to the removal of oxide inclusions in the ESR process [42]. Up to now, it has been widely accepted that non-metallic inclusion removal in the ESR process takes place predominantly at the stage of liquid metal films formation and subsequent collection into liquid metal droplets at the electrode tip, whereas the stage when metal droplets pass through the slag pool and the process in the liquid metal pool contribute in an extremely small manner (does not play an important role).

3 Evolution of different types of original inclusions during ESR

The process of consumable electrode manufacturing (such as ladle furnace (LF), vacuum degassing (VD), and Ruhrstahl–Heraeus (RH) refining) for ESR would give rise to the inclusions with different compositions and sizes, depending on liquid steel composition, slag chemistry, deoxidation schemes and activities of inclusion-forming species (typically soluble oxygen, aluminum, calcium, magnesium, silicon, sulfur, and nitrogen), heating scheme, vacuum, and stirring states. Different deoxidation schemes (deoxidizing agent chemistry, and its addition amount and timing) are employed for liquid steel deoxidation according to the requirements of individual steel grade when manufacturing the consumable electrode for ESR. Non-metallic inclusions with different chemical compositions basically experience various evolution trajectories during ESR. Furthermore, the removal degree (number proportion) of the original inclusions during ESR is also largely

dependent on the compositions and sizes of these inclusions, and other parameters (liquid metal and slag compositions, melting rate and capacity of ESR, etc.) have more or less influences on the original inclusion removal. In this section, the evolution of different types of inclusions (Al_2O_3, $MgO{\cdot}Al_2O_3$, calcium aluminate inclusions, manganese silicate inclusions, sulfide, and nitride inclusions) during ESR is assessed.

3.1 Oxide inclusion

3.1.1 Al_2O_3 and $MgO{\cdot}Al_2O_3$ inclusions

Alumina is the typical inclusion type in aluminum-killed steel. Part if not all of Al_2O_3 inclusions would be transformed to $MgO{\cdot}Al_2O_3$ inclusions provided that the steel contains several parts per million of soluble magnesium [1, 43–47]. These oxide inclusions frequently provide heterogeneous nucleation sites for primary carbides and nitrides, promoting their formation [48–50], which inevitably leads to similar detriments as Al_2O_3 and $MgO{\cdot}Al_2O_3$ inclusions to the steel.

In the present article, $MgO{\cdot}Al_2O_3$ inclusion represents both $MgO{\cdot}Al_2O_3$ spinel and low-MgO-containing $MgO{\cdot}Al_2O_3$ inclusion (with composition in the spinel + alumina two-phase region, namely the mixture of Al_2O_3 with very small amounts of $MgO{\cdot}Al_2O_3$ spinel [51]). As for original Al_2O_3 inclusions from the electrode, they would be converted to $MgO{\cdot}Al_2O_3$ inclusions in liquid steel after soluble magnesium pickup during the ESR. During the ESR without Mg-containing alloy addition, steel–slag reaction is the only potential source of soluble magnesium pickup in liquid steel. If the reduction of MgO from the slag by soluble species in liquid steel could take place, the dissolved magnesium originating from this source would be transported into the liquid steel and modify Al_2O_3 inclusions to $MgO{\cdot}Al_2O_3$ inclusions. Nevertheless, commercial slag for ESR contains low MgO content (much smaller than 5 mass%) and high Al_2O_3 content (higher than 20 mass%), and the reduction reaction between MgO in the slag and soluble species in liquid steel has to be critically assessed. The reaction between soluble aluminum in liquid steel and MgO in the slag is expressed as follows [52, 53]:

$$\begin{aligned} &2[\mathrm{Al}]+3(\mathrm{MgO}) = 3[\mathrm{Mg}]+(\mathrm{Al_2O_3}) \\ &\Delta G^{\mathrm{o}} = 980,685 - 328.486T\ (\mathrm{J/mol}) \end{aligned} \tag{1}$$

$$K=\frac{a_{\mathrm{Mg}}^3 \cdot a_{\mathrm{Al_2O_3}}}{a_{\mathrm{Al}}^2 \cdot a_{\mathrm{MgO}}^3} = \frac{\left(f_{\mathrm{Mg}} w_{[\mathrm{Mg}]}\right)^3 \cdot a_{\mathrm{Al_2O_3}}}{\left(f_{\mathrm{Al}} w_{[\mathrm{Al}]}\right)^2 \cdot a_{\mathrm{MgO}}^3} \tag{2}$$

where ΔG^{o} is the standard Gibbs free energy change; T is the temperature; K is the equilibrium constant; a_{MgO} and $a_{\mathrm{Al_2O_3}}$ are the activities of MgO and Al_2O_3 in the slag, respectively; a_{Mg} and a_{Al} are the activities of soluble magnesium and aluminum in liquid steel, respectively; $w_{[\mathrm{Mg}]}$ and $w_{[\mathrm{Al}]}$ are the mass percent of soluble magnesium and aluminum in liquid steel, respectively; and f_{Al} and f_{Mg} are the activity coefficients of soluble aluminum and magnesium in liquid steel, respectively, which can be calculated by Wagner formula [54].

Figure 1 shows the Gibbs free energy change for the reaction between MgO in the slag and the soluble aluminum in liquid steel against the soluble aluminum content in liquid steel. Slag A1 (30.4 mass% CaF_2, 28.7 mass% CaO, 30.7 mass% Al_2O_3, 2.5 mass% MgO, and 6.7 mass% SiO_2) is a typical slag used in ESR industrial production. Slag B1 (32.9 mass% CaF_2, 28.7 mass% CaO, 30.7 mass% Al_2O_3, 5 mass% MgO, and 1.7 mass% SiO_2) is designed in order to assess Reaction (1) at upper limit of MgO content. A tool steel with the chemical composition of C 0.41, Si 1.06, Mn 0.36, Cr 5.17, V 0.96, Mo 1.27, Ca 0.0017, Mg 0.0002, and O 0.0008 (in mass%) is used in the thermodynamic calculation. In consideration of possible higher temperatures of molten slag, 1800 °C is also employed for comparison as shown in Fig. 1.

The Gibbs free energy change for Reaction (1) was calculated in combination with the calculated activity coefficients and the reported interaction parameters [47, 52] as well as the estimated activities of slag components relative to pure solid standard states at 1600 and 1800 °C with FactSage 7.2 (FToxid database). Figure 1 shows that Reaction (1) cannot occur toward the right-hand side when the soluble aluminum content is lower than 0.075 mass% and the MgO content of the slag is lower than 5 mass% at 1800 °C for the case of 0.0002 mass% Mg in steel and 30.7 mass% Al_2O_3 in the slag. It is a universal

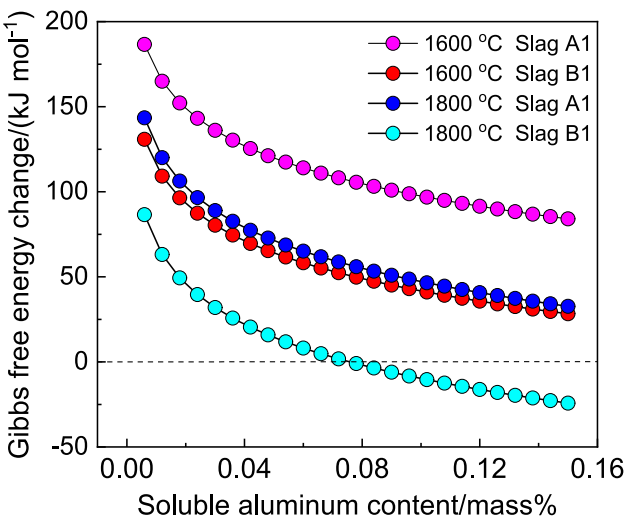

Fig. 1 Gibbs free energy change for reaction between MgO in slag and soluble aluminum in liquid steel against soluble aluminum content of liquid steel and MgO content of slag

fact that the MgO content is lower than 5 mass% in the slag for ESR. It suggests that steel–slag reaction cannot provide magnesium pickup in Al-killed steel during the ESR, let alone a lower aluminum content and the temperatures lower than 1800 °C. For this case, Al_2O_3 inclusions cannot be modified to $MgO{\cdot}Al_2O_3$ inclusions during the ESR process.

Al_2O_3 and $MgO{\cdot}Al_2O_3$ inclusions are stable in their compositions during the ESR without intentional alloy addition. The original Al_2O_3 and $MgO{\cdot}Al_2O_3$ inclusions in the electrode that have not been removed during the ESR would survive until in as-cast ingot [47, 55, 56]. The results from industrial-scale ESR trials on martensitic stainless steel in Ref. [57] indicate that the $MgO{\cdot}Al_2O_3$ inclusions from the electrode would survive in the ESR process according to the low amount of MgO in the slag (about 3 mass%) and the lack of refractory in the ESR. Survival of part of $MgO{\cdot}Al_2O_3$ inclusions from the consumable electrode were found in the electroslag remelting of Inconel 718 superalloy [58].

In view of the serious detriment of Al_2O_3 and $MgO{\cdot}Al_2O_3$ inclusions to the steel, besides maximizing Al_2O_3 and $MgO{\cdot}Al_2O_3$ inclusions removal from steel, modifying these inclusions to calcium aluminates with low melting temperature by calcium treatment is an alternative countermeasure to minimize their detriments to steel. The effectiveness and routes of calcium modification of alumina and $MgO{\cdot}Al_2O_3$ spinel inclusions have been confirmed by previous researchers in industrial steelmaking practices [52, 59–63] and laboratory-crucible experiments [52, 64–66]. In the case where $MgO{\cdot}Al_2O_3$ spinel is the only type of oxide inclusions in the steel electrode, all original $MgO{\cdot}Al_2O_3$ spinels in the electrode (except for that has been removed in the protective argon gas atmosphere ESR process) are modified to mainly CaO–MgO–Al_2O_3 and some CaO–Al_2O_3 inclusions during protective argon gas atmosphere ESR combined with a proper amount of online calcium addition, both of which have a low melting temperature and homogeneous compositions [67]. The modification of $MgO{\cdot}Al_2O_3$ spinel inclusions during ESR by calcium treatment is schematically represented in Fig. 2 [67]. The modification involves two routes, i.e., partially modified inclusion (the upper route in Fig. 2) and completely modified inclusion (the lower route in Fig. 2). It is the incomplete or complete reduction of MgO from $MgO{\cdot}Al_2O_3$ spinel by calcium that contributes to the modification of $MgO{\cdot}Al_2O_3$ spinels to CaO–MgO–Al_2O_3 and CaO–Al_2O_3 inclusions, respectively.

Simultaneous modification of alumina and $MgO{\cdot}Al_2O_3$ inclusions and its possible extent have been ascertained by Shi et al. [47]. Figures 3 and 4 illustrate the scanning electron microscopy (SEM) micrograph and element mappings of typical inclusions in steel after a proper amount of calcium addition during pilot-scale protective argon gas atmosphere ESR. It shows that calcium treatment modifies all $MgO{\cdot}Al_2O_3$ and alumina inclusions that have not been removed in the protective argon gas atmosphere ESR process to liquid/partially liquid CaO–Al_2O_3(–MgO) with uniformly distributed elements, in addition to a small proportion of partially modified inclusions of a CaO–MgO–Al_2O_3 core surrounded by an outer liquid CaO–Al_2O_3. Examples of partially modified oxide inclusions by calcium in the ingot are presented in Figs. 3c and 4. It has been confirmed that online calcium addition during the protective argon gas atmosphere ESR process indeed modify all alumina to liquid/partially CaO–Al_2O_3 inclusions with homogeneous compositions, as well as modified $MgO{\cdot}Al_2O_3$ inclusions to calcium aluminate inclusions. The mechanism of calcium modification has been proposed by these authors [47].

3.1.2 Calcium aluminate inclusions

It is more difficult to remove liquid calcium aluminate inclusions from liquid steel in comparison with solid oxide inclusions in liquid steel [68–72]. It is because the contact angle of liquid oxide inclusions in liquid steel is much smaller than 90°, which is a basic threshold whether the inclusion can be removed smoothly in liquid steel or not [73–76]. This is the case in the ESR of steel [77].

In the ESR of the steel in which CaO–Al_2O_3–SiO_2–1 mass% MgO is the only type of oxide inclusions (almost all of these inclusions have low melting temperature (< 1600 °C)), all original oxide inclusions that have not been removed are transformed to CaO–Al_2O_3–SiO_2–MgO with high melting temperature (> 1600 °C) in liquid metal pool [77]. It is that the reduction reaction of SiO_2 from the original oxide inclusions in the consumable electrode by soluble aluminum in liquid steel during ESR (i.e., $4[Al] + 3(SiO_2) = 3[Si] + 2(Al_2O_3)$) that results in the modification of oxide inclusion composition. This conclusion has been confirmed by thermodynamical calculation and inclusion composition analysis [77]. These modified oxide inclusions by steel reaction remain until in remelted ingot.

Except for the soluble species that are already contained in the steel, the species that are brought from alloy additions into liquid steel during ESR could also modify original oxide inclusion composition. Wang et al. [78] reported that original CaO–SiO_2–MgO–Al_2O_3 (with average composition of 13.6 mass%, 7.6 mass%, 2.6 mass%, and 35.2 mass% in order) in the H13 steel electrode were transformed to CaO–MgO–Al_2O_3 in liquid metal pool by the reduction of SiO_2 from the inclusion by soluble aluminum in laboratory-scale protective atmosphere ESR. Meanwhile, the MgO content in this type of oxide inclusions is

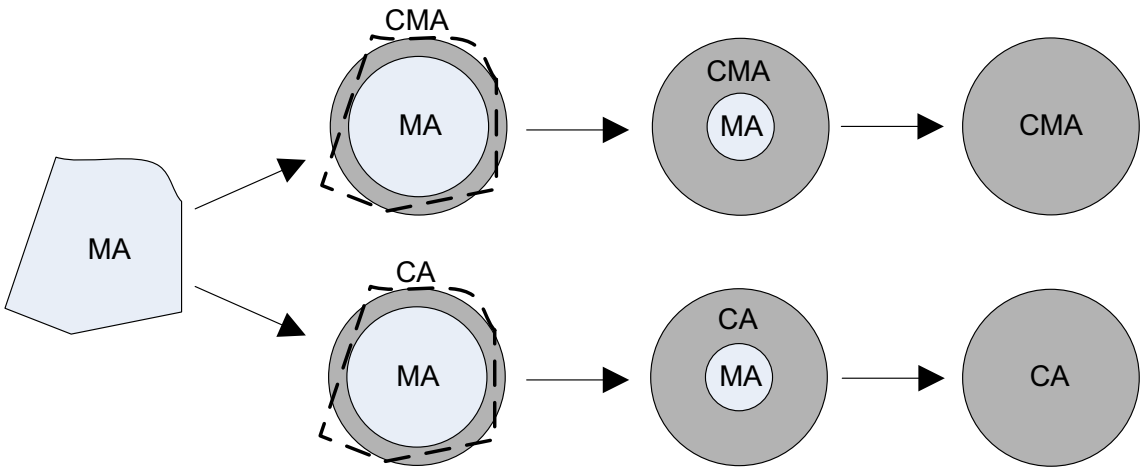

Fig. 2 Schematic diagram of $MgO{\cdot}Al_2O_3$ spinel inclusion modification by online calcium treatment in ESR process. C, M, and A stand for CaO, MgO, and Al_2O_3, respectively [67]

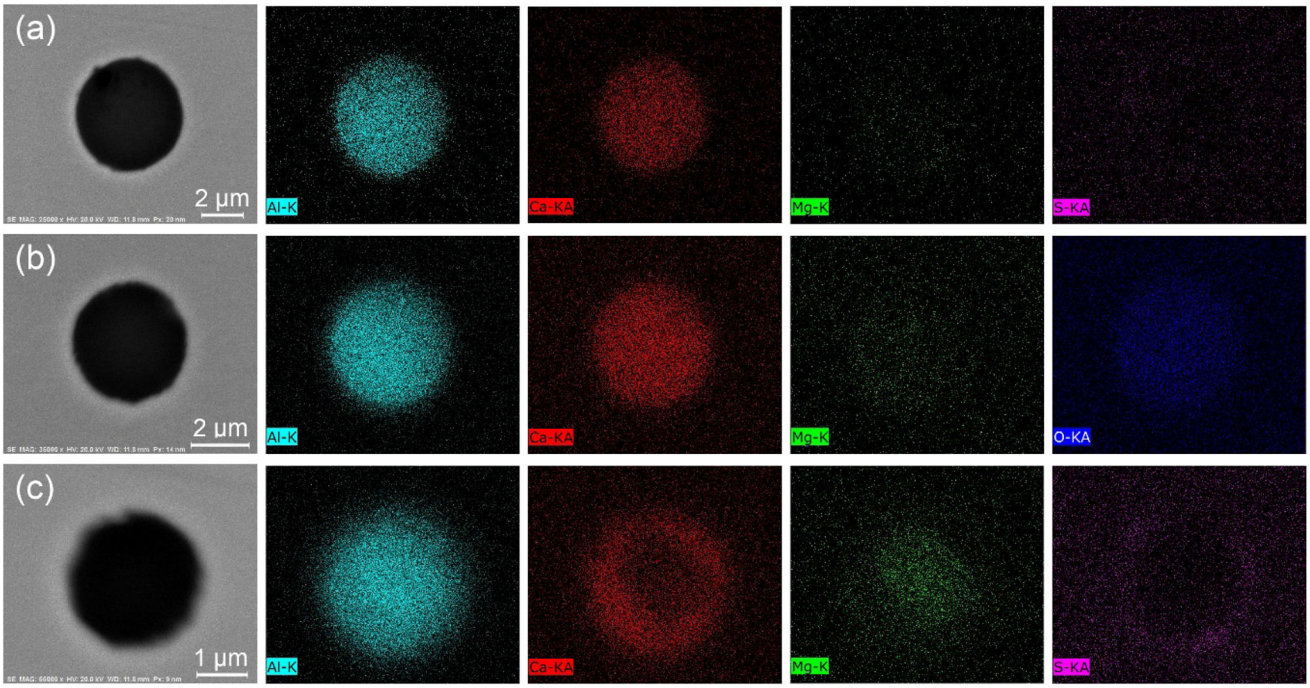

Fig. 3 Element mappings of typical inclusions observed in remelted ingot. **a** $CaO–Al_2O_3$; **b** $CaO–MgO–Al_2O_3$; **c** ternary-phased $CaO–MgO–Al_2O_3 + CaO–Al_2O_3 + CaS$ [47]

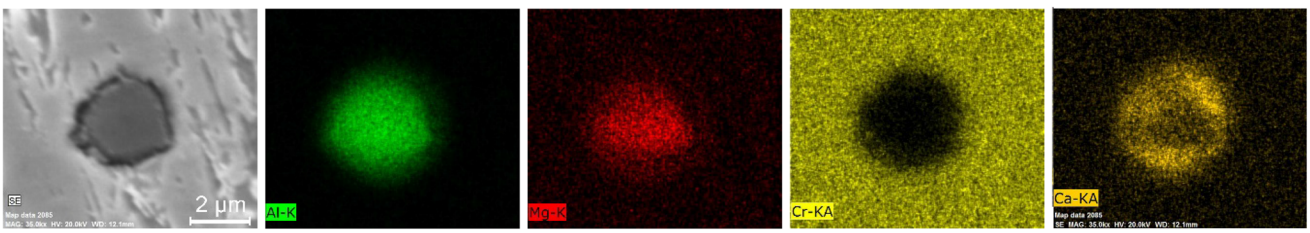

Fig. 4 Element mappings of a partially extracted inclusion in as-cast ingot. MgO and Al_2O_3 are enriched in core and poor at outside layer, and CaO shows opposite distribution [47]

increased to 10.3 mass% in liquid metal pool and 21.1 mass% in the remelted ingot. It is due to the modification reaction after 94.2 mass% Al–4 mass% Mg alloy addition during ESR, as expressed in Eq. (3) [78].

$$[\mathrm{Mg}] + (x\mathrm{CaO} \cdot y\mathrm{MgO} \cdot z\mathrm{Al_2O_3}) = (x\mathrm{CaO} \cdot (y+1)\mathrm{MgO} \cdot (z-1/3)\mathrm{Al_2O_3}) + 2/3[\mathrm{Al}] \quad (3)$$

The results from the laboratory-scale ESR trials on a tool steel electrode, in which the inclusions are mainly CaO–MgO–Al_2O_3–SiO_2 + (CaS), MgO–Al_2O_3–SiO_2, and Al_2O_3–SiO_2, show that almost all these original inclusions are removed during the ESR [79]. In a separate work, industrial-scale protective atmosphere ESR trials on bearing steel G20CrNi2Mo with a low oxygen content (0.0012 mass%) show that all original oxide inclusions (CaO–MgO–Al_2O_3 (with melting temperature lower than 1600 °C) and the complex inclusions of MgO·Al_2O_3 core surrounded by an outer CaO–Al_2O_3 layer) are removed in two ways, i.e., most of them are absorbed by the molten slag, and the others are dissolved into liquid steel [26]. Even the elimination of these original calcium aluminate inclusions is the case, these complex inclusions of MgO·Al_2O_3 core surrounded by an outer CaO–Al_2O_3 layer cannot be removed by dissolution into liquid steel. More research is needed to reveal the evolution of calcium aluminate inclusions with different compositions during ESR and ascertain the steel and slag composition conditions for maximal removal of these inclusions.

3.1.3 Manganese silicate inclusions

Manganese silicate inclusion is the main type of oxide inclusions in Si–Mn deoxidized steel. These inclusions are generally in liquid state at steelmaking temperatures [80–82]. Figure 5 shows the composition distribution of the inclusions detected in a Si–Mn-killed steel on ternary MnO–SiO_2–Al_2O_3 phase diagram.

Figure 5 shows that around half of these oxide inclusions are in liquid state at the temperatures lower than 1500 °C. 92.6% of the inclusions is smaller than 8 μm in the relative fraction of the number. It has been confirmed that all MnO–SiO_2–Al_2O_3 inclusions are removed through the dissociation of a portion of these original oxide inclusions into liquid steel and the absorption of the others by the molten slag during the ESR process [83]. Similar finding has been reported by Liu et al. [84] for the original MnO–SiO_2–Al_2O_3 inclusion evolution in low-aluminum steel electrode in laboratory-scale ESR trials. The oxide inclusions are mostly MgO·Al_2O_3 containing about 3 mass% MgO both in the liquid metal pool and in the remelted ingots, and the others are Al_2O_3 inclusions. Nearly all these inclusions readily formed in the liquid

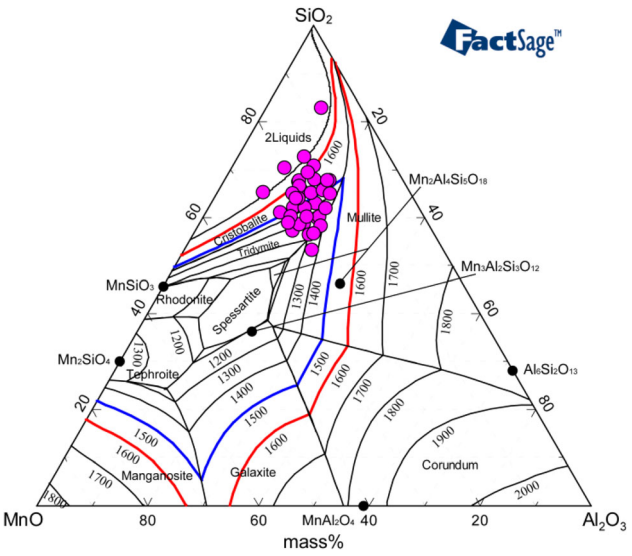

Fig. 5 Composition distribution of oxide inclusions in steel electrode on MnO–SiO_2–Al_2O_3 ternary phase diagram (temperature in degree Celsius). Pink solid circles represent compositions of inclusions, and some of these pink solid circles overlap each other [83]

metal pool as a result of the reactions between alloying elements and the soluble oxygen in liquid steel that dissociated from MnO–SiO_2–Al_2O_3 inclusions, and the others formed during the solidification of liquid steel in the mold [83].

3.2 Sulfide inclusion

It is during solidification of liquid steel that sulfide inclusions are formed in the manufacture of the electrode, except for high-sulfur steel. The removal and formation of sulfide inclusions during the ESR are closely related to the desulfurization of liquid steel [33]. Desulfurization in electroslag remelting is not a heavy load in comparison with other tasks of ESR, such as deoxidation, non-metallic inclusion removal, lowering the loss of alloying elements and retardation of segregation.

Sulfide inclusion removal during ESR is documented in Refs. [21, 25, 47, 55, 67, 77, 85], which confirm full elimination of sulfide inclusions from the electrodes during the ESR. It is demonstrated that the removal of (Mn,Cr)S inclusions during ESR process is attributed to the dissolution of sulfide inclusions into soluble sulfide-forming elements into liquid steel taking place at the electrode tip during liquid metal films formation and their collection into droplets [55]. The removal mechanism of (Mn,Cr)S inclusions described by Liu et al. [25] is in accordance with that in Ref. [55]. Later, the removal of MnS and CaS inclusions is confirmed to be in a same route [21, 47, 67, 85].

The soluble sulfur in liquid steel that dissociates from the original sulfide inclusions could be removed by the desulfurization reaction. Note that no sulfide inclusions are found in the liquid metal pool [47, 77]. Like that in continuous casting and mold casting, sulfide inclusions are frequently formed during liquid steel solidification in the ESR. These newly formed sulfide inclusions could hardly be removed in the ESR. The types of these sulfide inclusions could be same as those in the electrode or different from those in the electrode [21, 47, 77]. The sulfide inclusions in the remelted ingot originate from the following sources:

(1) During liquid steel solidification in the ESR, single-phase sulfide precipitates at the solidification front due to local enrichment of soluble sulfur and manganese in residual liquid phase once the solid fraction is greater than the critical value [25, 86]. As an example, MnS inclusion precipitates in NiCrMoV alloy as a function of the product of $w_{[Mn]} \times w_{[S]}$ and the solid fraction has been confirmed to be in this way as shown in Fig. 6 [25].

(2) During cooling and solidification of liquid steel in the ESR, two types of oxide–sulfide complex inclusions according to the morphology of sulfide around calcium aluminate inclusion are formed, i.e., shell-type CaS and patch-type CaS [77, 85]. Examples of these two types of oxide–sulfide complex inclusions are presented in Figs. 7 and 8 [85]. It has been confirmed in Ref. [85] that the shell-type CaS in the oxide–sulfide complex inclusion is formed as a result of the reaction between CaO in the liquid $CaO–Al_2O_3–SiO_2–MgO$ inclusion and soluble aluminum and sulfur in liquid steel until the solid fraction of liquid steel exceeds 0.34 during the industrial-scale ESRR process, and the formation of patch-type CaS in the oxide–sulfide complex inclusion originates from decreasing solubility of CaS in $CaO–Al_2O_3–SiO_2–MgO$ inclusion melt during the cooling of liquid steel in the electroslag rapid remelting (ESRR) process.

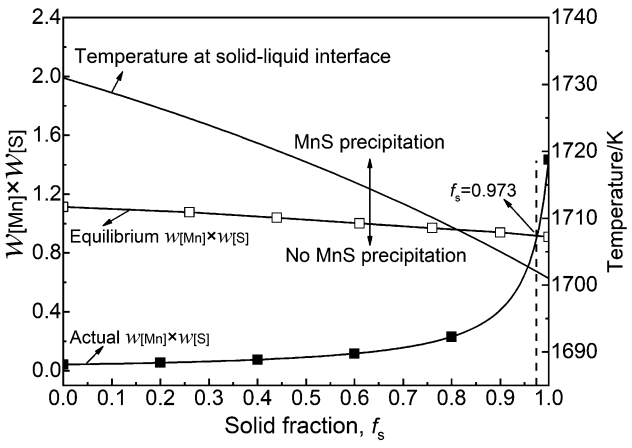

Fig. 6 Relationship between equilibrium concentration product of [Mn] and [S] and solid fraction for MnS inclusion formation in transition zone of dual alloy NiCrMoV and CrMoV [25]

The desulfurization degree of ESR influences the generation of new sulfide inclusions during the ESR, in which a higher desulfurization efficiency would suppress the generation of fresh sulfide inclusions. Furthermore, increasing the cooling rate of ESR could retard the nucleation and growth of sulfide inclusions. The suppression of MnS inclusion formation in terms of its size and number density during liquid steel solidification by increasing the cooling rate of ESR has been confirmed by pilot-scale ESR trials [86]. However, more study is needed to clarify the mechanism of effects of cooling rate on sulfide inclusions through its role on the segregation of sulfide-forming elements during liquid steel solidification, undercooling and the time for nucleation and growth of sulfide inclusion.

3.3 Nitride inclusion

The elimination of AlN inclusions in the electrode during the ESR of high-Al steel (1 mass% Al and 0.0032 mass% N) is attributed to their dissolution into liquid steel as soluble aluminum and nitrogen taking place at the electrode tip during liquid metal films formation and their collection into droplets [87]. The thermodynamic calculation shows that AlN inclusions are unable to precipitate in the liquid metal pool. During the solidification of liquid steel, Al and N would enrich in the residual liquid phase between dendritic arms at solidification front with the increase in solid fraction. The relationship between the concentration product $w_{[Al]} \times w_{[N]}$ for AlN precipitation and the solid fraction, as well as the calculated critical value at the liquidus temperature is shown in Fig. 9. The presence of AlN inclusions in remelted ingot originates from their precipitation in the residual liquid phase at the solidification front where the solid fraction is greater than the calculated critical values caused by the local enrichment of soluble Al and N. These AlN inclusions formed in interdendritic liquid steel could hardly be removed by floating up [40, 41]. Huang et al. [88] have also confirmed that TiN and VN inclusions are unable to precipitate above the liquidus temperature of H13 tool steel containing 0.052 mass% Ti, 0.84 mass% V, and 0.0089 mass% N.

Formation of fresh nitride inclusions generally cannot take place in liquid metal pool during ESR. Nevertheless, for electroslag remelting of high-Ti/low-N alloy, it has been confirmed that part of original TiN inclusions dissociated into soluble Ti and N in liquid alloy at the electrode tip, and the dissociation of the others into soluble Ti and N

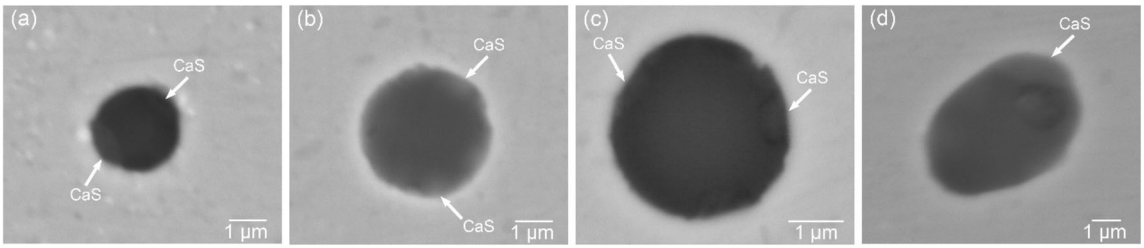

Fig. 7 CaO–Al_2O_3–SiO_2–MgO inclusion associated with patch-type CaS in remelted ingots. Arrows indicate some of patch-type CaS in a complex inclusion [85]

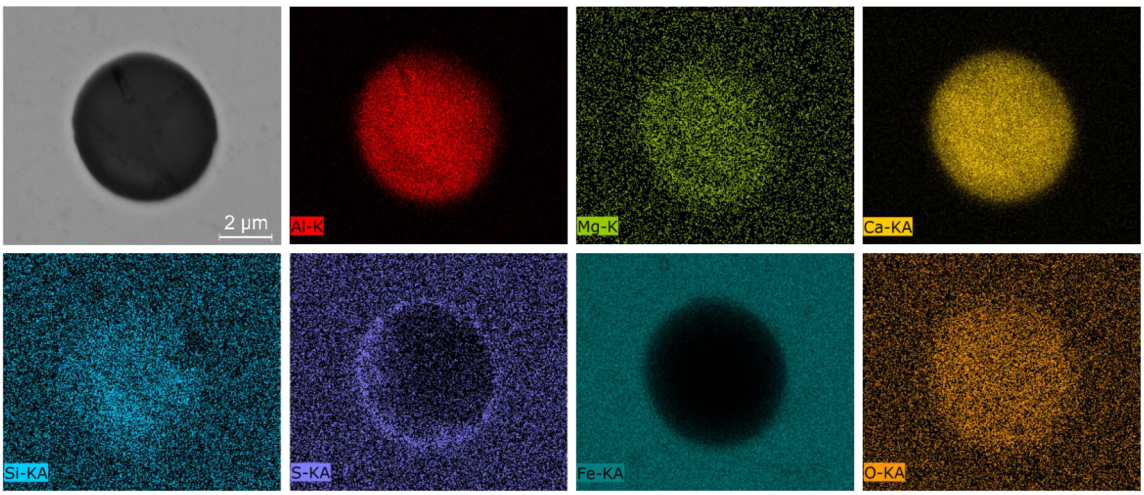

Fig. 8 Element mappings of shell-type CaS associated with CaO–Al_2O_3–SiO_2–MgO inclusion in remelted ingot [85]

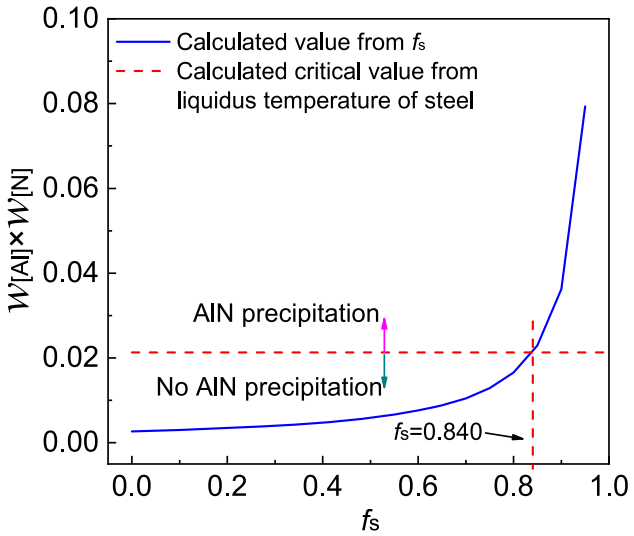

Fig. 9 Relationship between concentration product $w_{[Al]} \times w_{[N]}$ and solid fraction for AlN inclusion precipitation [87]

in the liquid alloy took place when liquid metal droplets passed through the molten slag pool and in the elevated temperature region of the liquid metal pool. TiN inclusions in remelted ingots were mainly generated in liquid metal pool during ESR, and the others were formed during the solidification of liquid alloy (taking up a small proportion) [89].

The calculated results based on a kinetic model indicate that the full dissolution of a TiN inclusion with 6 μm in Ni–22Cr–12Co nickel-based superalloy (0.44 mass% Ti and 0.0028 mass% N) is completed in 1.17 s [90]. It is deduced in Ref. [90] that all original TiN inclusions are removed through their dissolution during the ESR, and the TiN inclusions in the remelted ingot are those precipitated during solidification of liquid alloy. A thermodynamic calculation is still needed to assess the dissolution of TiN inclusions in this work.

Figure 10 shows the distribution of TiN particles near a slag inclusion and an example of a TiN cuboid with a $MgO{\cdot}Al_2O_3$ core in an industrial-scale ingot produced by ESR. A large number of cuboid TiN inclusions are present in the INCOLOY alloy 800 and 825 electrode with similar size and morphology to those observed surrounding slag inclusions in the ingots. Busch et al. [91] proposed that the TiN particles in the ingots are relics from the electrode production process. The evolution of these TiN particles from the electrode to remelted ingot could be validated according to thermodynamic calculation and kinetic analysis.

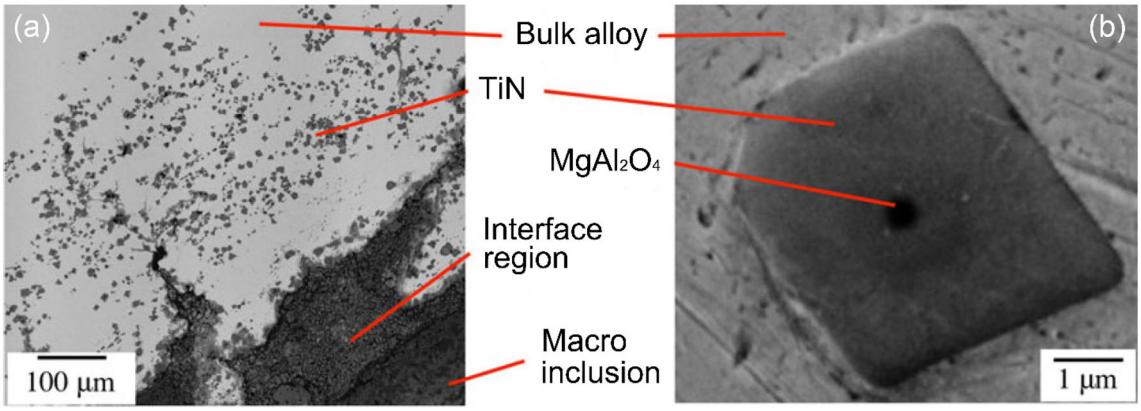

Fig. 10 SEM micrographs of TiN particles. **a** TiN particle distribution near a slag inclusion; **b** TiN cuboid with a $MgAl_2O_4$ core [91]

4 Role of processing parameters of ESR on inclusions

4.1 Deoxidation schemes of ESR

The iron oxide activity of the slag is a measure of its oxygen potential during ESR [24, 92–94]. Although it is a fact that the FeO content of the slag throughout the ESR process is much lower than 1 mass% in the production practice [55, 95–97], the FeO content of the molten slag is indeed far higher than the equilibrium value [85]. The oxygen level of Al-killed steel is determined by [Al]–[O] equilibrium during the ESR, whereas FeO in the slag transfers oxygen into the liquid steel even though the measured FeO content is very low (0.4 to 0.6 mass%) in the slag [85]. To this end, the intention of deoxidizing agent addition in the ESR is to deoxidize the molten slag [24, 55, 92, 93, 98–100]. In parallel, it is inevitable in most cases that deoxidizing agent would penetrate into the liquid steel and directly deoxidize the liquid steel [55]. The deoxidation of ESR and deoxidation-related processing parameters have been discussed in a recent review [32].

The interactions of atmosphere–slag–metal–inclusion system determine the deoxidation during the ESR of steel. The slag with a high oxygen potential would transfer oxygen into liquid steel, resulting in the generation of new oxide inclusions during the ESR process. The study by the present authors did show that new $CaO–Al_2O_3–MgO$, $MgO·Al_2O_3$, and $CaO–Al_2O_3–MgO–SiO_2$ inclusions are formed by the reactions taking place inside liquid metal pool as reoxidation products [77]. In addition, transformation of original semiliquid $CaO–Al_2O_3–MgO$ inclusions to liquid $CaO–Al_2O_3–MgO–SiO_2$ inclusions as a result of the reaction between these original inclusions, the dissolved oxygen supplied from the FeO in slag and concerned elements in liquid steel has been confirmed in protective Ar gas atmosphere ESRR of the steel with a low oxygen concentration (0.0008 mass%) [85].

It is still a challenge to prevent oxygen introduction from the atmosphere and FeO in the slag even though protective inert atmosphere is employed in the ESR production. In the family of ESR technologies, vacuum electroslag remelting exhibits a particular advantage in prevention of oxygen introduction [101]. The ESR refining in vacuum atmosphere (0.01 MPa) brings lower oxygen content of H13 steel in comparison with argon atmosphere ESR (0.1 MPa) because of carbon deoxidization in vacuum atmosphere [88], which consequently lowers the size and number of inclusions.

Slag deoxidation of ESR not only determines the oxygen level of liquid steel, but also influences the concentrations of oxide inclusion-forming species in liquid steel. Laboratory-scale electroslag remelting of 4340 steel using 50% CaF_2–40% CaO–10% Al_2O_3 slag was performed by Reyes-Carmona and Mitchell [92], showing that Ca-deoxidizing agent addition above critical addition rate 10 kg/t gives a low FeO activity of the slag, high aluminum content and aluminates in remelted ingot caused by the reaction between calcium and Al_2O_3 in the slag.

In the case of Si–Ca and Al deoxidizing agents for the deoxidation of 316L stainless steel during the industrial-scale ESR, the inclusions in the remelted ingot are $MgO·Al_2O_3$, $CaO–MgO–Al_2O_3$, $MgO·Al_2O_3$ core surrounded by a $CaO–Al_2O_3$ layer. However, $CaO–MgO–Al_2O_3–MnO$ and $CaO–Al_2O_3–SiO_2$ inclusions are generated because of Si–Ca and Al–Si–Mn alloy addition for the deoxidation during the ESR, besides $MgO·Al_2O_3$ and $CaO–MgO–Al_2O_3$ [102]. It is because Al–Si–Mn alloy addition introduces extra Mn and Si into liquid steel for oxide inclusion formation.

Al and Ca–Si are most commonly used deoxidizing agents for the deoxidation in the ESR. Some of the species from the deoxidizing agent pickup more or less in liquid

steel could hardly be avoided during the slag deoxidation of ESR, as well as an increase in other alloying elements in liquid steel through steel–slag reaction because of excessive deoxidizing agent addition [55, 67, 87, 100, 103–105]. These species would modify oxide inclusion composition during the ESR through steel–inclusion reaction for many cases. The slag deoxidation of laboratory-scale ESR using Al–Mg alloy demonstrated that the aluminum content increases from 0.0003 mass% in the electrode to 0.41 mass% in remelted ingot after 94.2 mass% Al–4 mass% Mg alloy addition for deoxidation of liquid steel during ESR [84]. Consequently, the calcium content is increased because of the reduction of CaO from the slag by aluminum (0.41 mass%), and fresh CaO–Al_2O_3–MgO and CaO–Al_2O_3 inclusions in liquid steel form, leading to an increase in the proportions of CaO–Al_2O_3–MgO and CaO–Al_2O_3 inclusions and the CaO content of oxide inclusions [84].

An increase in the Al_2O_3 content in the complex oxide inclusions as a result of the increase in the aluminum content of liquid steel because of excessive addition rate of deoxidizing agent aluminum during the ESR has been demonstrated in Ref. [92]. Nevertheless, this is not always the case. In electroslag remelting of H13 tool steel with $MgO{\cdot}Al_2O_3$ spinels as the only oxide inclusions, significant soluble aluminum pickup in liquid steel did not cause the modification of the composition and size of the original oxide inclusion that have not been removed during the ESR [67]. A same conclusion was drawn for electroslag remelting of a corrosion resistant die steel, in which Al_2O_3 is the only type of oxide inclusion [55].

4.2 Slag composition

The elimination of oxide inclusions during the ESR is attributed to their dissolution into the slag phase, except for that dissociated in its individual chemical species into liquid steel. The loss of tantalum during protective argon atmosphere laboratory-scale ESR of a Ta-containing martensitic steel is the focus of the study in Ref. [106], and Ta-containing precipitated phase and the number density of inclusions were identified as shown in Fig. 11 in combination with slag chemistry analysis, which demonstrates that 95% reduction in number density of Ta_2O_5 inclusions during the ESR results in 25% loss of Ta and an increase of the Ta_2O_5 content by 1.66 mass% in the slag. Slag chemistry generally exerts a pronounced influence not only on the inclusion removal, but also on the modification of oxide inclusion composition in the ESR process [40, 107–109]. Note that the role of slag chemistry on the modification of oxide inclusion composition is accomplished through steel–slag reactions and steel–inclusion reactions.

The driving force for steel–inclusion reaction is the difference in oxide activities between the slag and oxide inclusions. It is the steel–slag reaction, by affecting the element content in liquid steel that contributes to the compositional modification of oxide inclusions during ESR. The MgO content in $MgO{\cdot}Al_2O_3$ inclusions in laboratory-scale remelted ingot is found to increase with increasing the CaO content of the slag from 8 to 20 mass% for ESR [110]. It originates from that the activity of SiO_2 in slag is lowered by increasing the CaO content of the slag, leading to an increase in the Mg content of liquid steel according to the steel–slag reaction $[Si] + 2(MgO) = (SiO_2) + 2[Mg]$.

ESR slags are CaF_2–CaO–Al_2O_3-based system with minor additions of MgO, TiO_2 and/or SiO_2 to tailor the slag for the specific remelting requirements. The slag is generally required to minimize the SiO_2 content for ESR of alloy and steel. However, it has been demonstrated that a certain amount of SiO_2 has to be added in the slag for ESR of some varieties of steels in order to prevent loss (or pickup) of silicon and aluminum in liquid steel and poor surface quality of as-cast remelted ingot [111–113].

The laboratory-scale ESR trials on low-alloy steel using the slag (31–55 mass% CaF_2, 0–30 mass% Al_2O_3, and 15–46 mass% CaO) with different SiO_2 contents (0–23 mass%) show that the slag with low SiO_2 content brings alumina or low-calcium aluminates as predominant inclusion type in the remelted ingot, and the SiO_2 content of the oxide inclusions increases as the SiO_2 content of the slag is increased, giving rise to aluminosilicate inclusions [93]. It is indeed the eventual direction that the evolution of oxide inclusion chemistry will come close to the chemical composition of the slag [109, 114], because steel–slag reaction and steel–inclusion reaction would continue towards equilibrium state until the ratios of the activities of the species are equal in the slag and oxide inclusions.

The variation of some components contents of the slag could restrain steel–slag reaction, which would retard steel–inclusion reaction for oxide inclusion composition evolution. It has been demonstrated in Ref. [77] that the SiO_2 content in liquid CaO–Al_2O_3–SiO_2–MgO inclusions is obviously lowered because of the reduction of SiO_2 from the original oxide inclusions by dissolved Al in liquid steel during the ESR, whereas this reduction of the SiO_2 content from the oxide inclusions becomes less marked originating from considerably decreasing Al pickup in liquid steel caused by increasing SiO_2 content in the slag, which retards the steel–slag reaction. In parallel, the oxide inclusions newly formed during the ESR possess a higher SiO_2 content in the case of the remelting with the higher SiO_2-containing slag [115].

The slag composed of 70 mass% CaF_2–30 mass% Al_2O_3 is a typical ESR-type slag, which has been widely used for

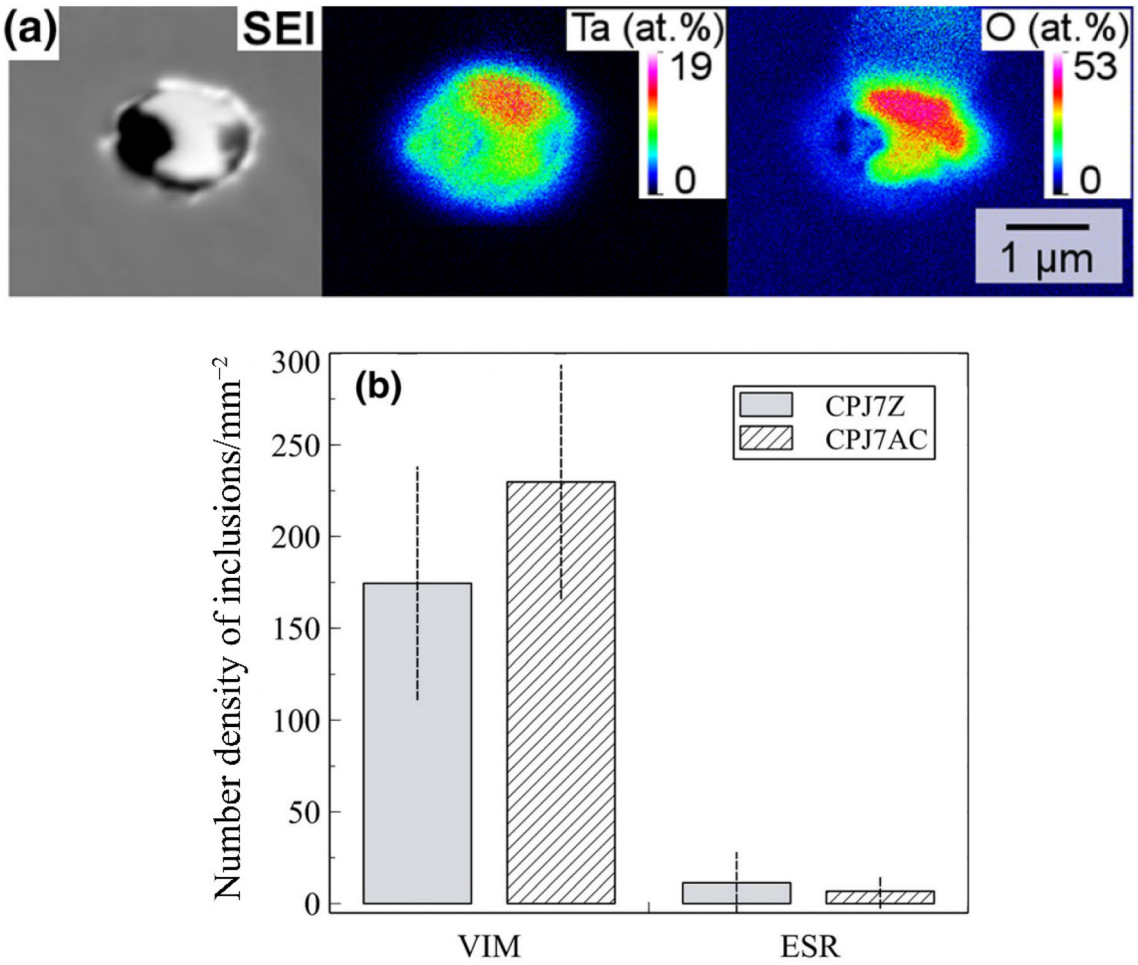

Fig. 11 Element mappings of a Ta_2O_5 inclusion by electron probe microanalysis (**a**) and number density of inclusions in martensitic steel CPJ7Z and CPJ7AC produced by vacuum induction melting (VIM) and ESR (**b**) [106]

several decades in the ESR industrial production. The study by Dong et al. [79] shows that almost all inclusions are Al_2O_3 in the ingot remelted under the 70 mass% CaF_2–30 mass% Al_2O_3 slag, whereas the inclusions are $MgO{\cdot}Al_2O_3$ spinels when using the multi-component slag (50 mass% CaF_2–20 mass% CaO–20 mass% Al_2O_3–5 mass% SiO_2–5 mass% MgO) in the laboratory-scale ESR, and nearly all original inclusions (CaO–MgO–Al_2O_3–SiO_2 + (CaS), MgO–Al_2O_3–SiO_2, and Al_2O_3–SiO_2) are removed during ESR in these two cases. The classification of non-metallic inclusions in the electrode and the remelted ingots is shown in Fig. 12 [79]. These two slag systems do not show a noticeable difference in the capacities for removal of original non-metallic inclusions.

In the ESR production practice, Al_2O_3 is an indispensable component in almost all commercial slag systems (basically around 30 mass% in its content). When Al_2O_3 in slag would exert an effect on the oxide inclusion composition, it would change the contents of the species in liquid metal first (usually soluble aluminum, silicon and oxygen) by slag–steel reaction, and then indirectly modify inclusion composition by steel–inclusion reaction. The results of laboratory-scale ESR trials in Ref. [116] indicate that almost all of the detected inclusions are Al_2O_3-type with minor contents of MgO or CaO in the ingot remelted with the 68 mass% CaF_2–30 mass% Al_2O_3–2 mass% SiO_2 slag.

Protective nitrogen gas atmosphere laboratory-scale ESR trials of bearing steel 100Cr6 with 0.0008 mass% of oxygen, in which the oxide inclusions are low-MgO-containing Al_2O_3–SiO_2–MgO and MgO–SiO_2, were performed by Schneider et al. [117, 118] in order to reveal the effect of the Al_2O_3 content in the slag on inclusions. In the case of remelting with Al_2O_3-free slag, the inclusions in the ingot are MgO-enriched SiO_2–MgO. Almost all inclusions are Al_2O_3 in the ingot produced by ESR using the slag containing 33 mass% of Al_2O_3, and low-Al_2O_3-containing slag (6 mass%) gave MA spinel inclusions in the ingot. It is attributed to the increased aluminum and oxygen contents of the steel, mainly resulting from the decomposition of Al_2O_3 caused by the increase in the Al_2O_3 content of the

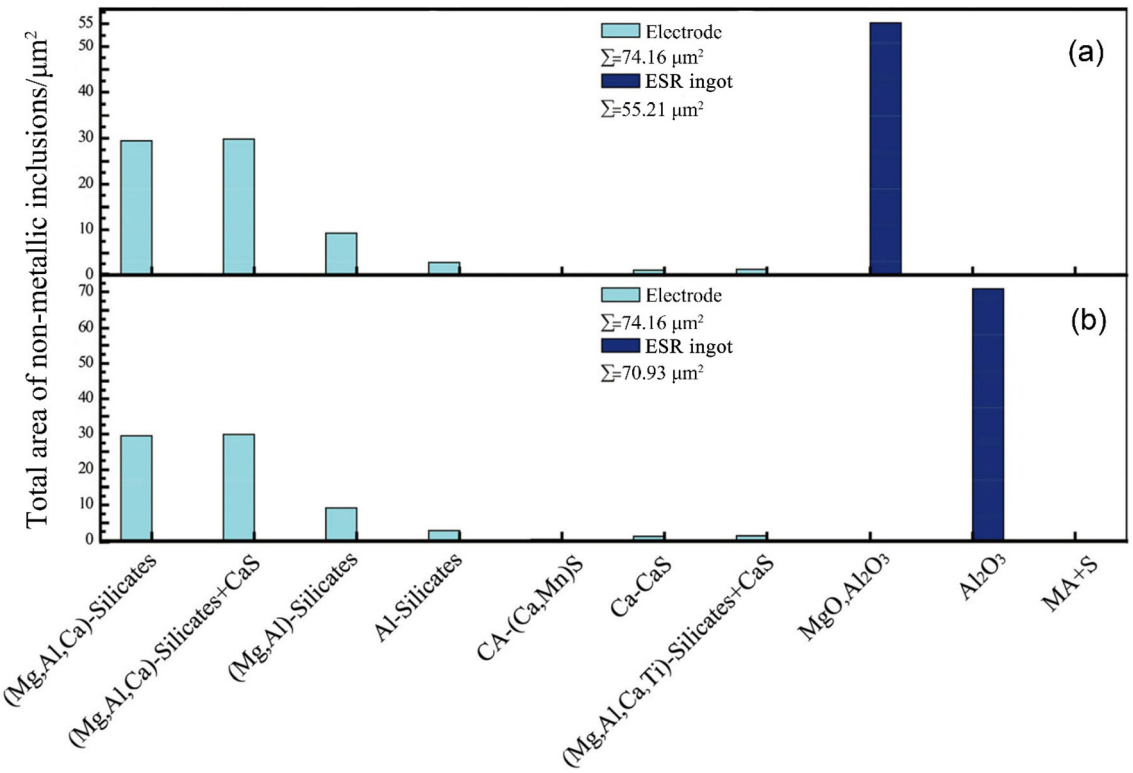

Fig. 12 Classification of non-metallic inclusions in electrode and remelted ingots. **a** Ingot remelted using slag composed of 50 mass% CaF_2–20 mass% CaO–20 mass% Al_2O_3–5 mass% SiO_2–5 mass% MgO; **b** ingot remelted using slag composed of 70 mass% CaF_2–30 mass% Al_2O_3 [79]

slag [117, 118]. Note that the oxygen content of steel is increased by twice to eight times after ESR in the above work by Schneider et al. [117, 118]. Therefore, reoxidation of liquid steel could also modify the compositions of these inclusions. It should be stressed that the decomposition of Al_2O_3 from the ESR-type slag could take place or not is a critical issue.

In industrial-scale ESR of the bearing steel G20CrNi2Mo, the oxide inclusions are CaO–MgO–Al_2O_3 (most of which are larger than 5 μm and in low-melting-temperature region (< 1600 °C)) of CaO–MgO–Al_2O_3 phase diagram and MgO–Al_2O_3 surrounded by an outer CaO–Al_2O_3 layer. The results show that all these original oxide inclusions have been removed in ESR. In the case of the slag with lower CaO content (4.42 mass%) and MgO content (0.1 mass%), most of the inclusions are Al_2O_3, and the others are Al_2O_3-riched CaO–Al_2O_3 and MgO–Al_2O_3 in the remelted ingot. In contrast, in the remelted ingots produced by ESR using the slag with higher CaO and MgO contents, the inclusions are MgO–Al_2O_3, CaO–Al_2O_3 and CaO–MgO–Al_2O_3, in which the CaO and MgO contents are higher arising from increased soluble calcium and magnesium contents in liquid steel [97].

Electroslag remelting of Q235B steel with low Al content (< 0.004 mass%) using the slag composed of 30 mass% CaF_2–44 mass% Al_2O_3–20 mass% CaO–6 mass% MgO shows that the oxide inclusions change from SiO_2–MnO in the electrode to Al_2O_3–MnO during the ESR process resulting from the transfer of aluminum from the slag to liquid steel [119]. The oxidation inclusion evolution is schematically illustrated in Fig. 13 [119]. As proposed in Ref. [119], it is the constant transfer of aluminum from the slag phase to liquid steel during ESR process that results in the increase in the aluminum content of the steel and the reaction between MnO and SiO_2 in inclusions and the

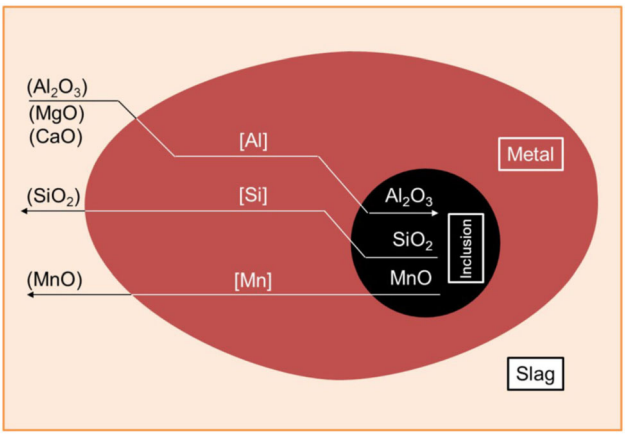

Fig. 13 Possible evolution mechanism of oxide inclusions during ESR of low aluminum Q235B steel [119]

soluble aluminum in liquid steel to generate Al_2O_3 in the inclusions. Herein, it is critical to assess the aluminum transfer from the slag to liquid steel according to steel–slag reaction.

For electroslag remelting of FGH96 superalloy with MgO–Al_2O_3 as the only oxide inclusions, the oxide inclusions in the laboratory-scale remelted ingots are transformed from MgO–Al_2O_3 to MgO–Al_2O_3–Ce_2O_3 and Al_2O_3–(69–73 mass%) Ce_2O_3 inclusions with increasing the CeO_2 content from 0 to 5 mass% and decreasing the Al_2O_3 content from 20 to 1 mass% in the slag. The change in the oxide inclusion composition is attributed to the reduction of MgO from the MgO–Al_2O_3 by soluble Ce in liquid metal, caused by the increased Ce content in the liquid metal originating from the reduction of CeO_2 from the slag by soluble aluminum in liquid metal [56].

As discussed above, the variation of slag chemistry usually induces the change in the chemical compositions of oxide inclusions in the ESR. However, this is not always the case. Zhou et al. [120] experimentally proved that almost all oxide inclusions are always Al_2O_3 in the ingots when increasing the SiO_2 content from 0 to 25 mass% in the slag for industrial-scale ESR of Al-killed bearing steel. The laboratory-scale electroslag remelting of Fe–25Ni–15Cr–2.8Ti alloy indicates that increasing the TiO_2 contents from 5.66 to 17.69 mass% in the slag has no influence on the oxide inclusion compositions in remelted ingots [89].

The desulfurization degree of the laboratory-scale pressurized nitrogen atmosphere ESR is confirmed to be lower than that of laboratory-scale open air atmosphere ESR because the low oxygen potential under N_2 pressure retards the gasifying reaction of sulfur in slag [121]. It has been demonstrated that the addition of 2 and 4 mass% Na_2O in the 60 mass% CaF_2–20 mass% CaO–20 mass% Al_2O_3 slag enhances the desulfurization degree of pressurized electroslag remelting in nitrogen atmosphere, which lowers the negative effect brought by pressurized nitrogen atmosphere on the desulfurization. Pressurized electroslag remelting is recognized as a promising technology for producing high nitrogen steel [121]. The role of Na_2O-containing slag and pressurized atmosphere of ESR on oxide inclusions has not been studied in published literature yet. Thus, future work is quite needed on this topic.

4.3 Melting rate of ESR

Liquid metal films form at the electrode tip and then collect into liquid metal droplets during ESR. Melting rate of the electrode in ESR (usually termed as melting rate of ESR) largely determines the thickness of liquid metal films and their residence time at the electrode tip [122, 123], as well as pool depth, the local solidification time and solidification rate of liquid metal [124–127], and consequently determines the residence time of inclusions in liquid metal. Non-metallic inclusions removal in the ESR process takes place predominantly at the stage of liquid metal films formation and subsequent collection into liquid metal droplets at the electrode tip, as well as liquid metal pool (more or less contribution). Therefore, it seems that increasing the melting rates of ESR is unfavorable to inclusion removal.

The removal effectiveness of CaO–Al_2O_3–SiO_2 inclusions in 316LC stainless steel during laboratory-scale ESR using 33.3 mass% CaF_2–33.3 mass% Al_2O_3–33.3 mass% CaO has been compared in terms of different melting rates of the electrode. The amounts of inclusions and oxygen in the ingot increase with increasing the melting rate of laboratory-scale ESR from 0.7, 0.9 to 1.2 kg/min. Ahmadi et al. [126] attributed this increase in the inclusion amounts to the increase in the speed of liquid metal droplets passing through the slag pool as the melting rates were increased, resulting in a decrease in the elimination of oxide inclusions. However, this deduction is open to question.

The effect of three different melting rates (at an interval of 100 kg/h) of protective atmosphere ESR on the inclusions in X12CrNiMoV12-3 steel deoxidized with Al was studied by Korp and Kubin [128] for producing an industrial-scale ingot with diameter of 750 mm. Melting rates have no influence on the types of oxide inclusions, which are Al_2O_3 and oxysulfide (main types), calcium aluminate, $MgO{\cdot}Al_2O_3$ and $MnO{\cdot}Al_2O_3$ before and after ESR. The increase in the melting rates of ESR results in an increase in the inclusion area proportion. Korp and Kubin [128] attributed the increase in the inclusion amount to an increase in the dissolved oxygen content of liquid steel as a result of the dissolution of oxide inclusions at electrode tip and possible source of SiO_2 dissolution from the slag, which is caused by the increase in the process temperature in ESR when increasing the melting rates. However, this deduction is lack of thermodynamic calculation for assessing the dissolution of original oxide inclusions and SiO_2 from the slag.

The variation of the melting rates of ESR does not necessarily make a difference in inclusions in the ESR and ingot, even if in a large-scale change. Melting rates (350, 400, 450, and 500 kg/h) of industrial-scale protective atmosphere electroslag rapid remelting exert a negligible effect not only on the steel cleanliness and the removal efficiency of CaO–Al_2O_3–MgO (27.5–40.3 mass% CaO, 36.4–52.0 mass% Al_2O_3, and 14.9–19.6 mass% MgO (a small amount (< 2 mass%) of SiO_2 is detected in some cases)) inclusions, but also on the inclusion size distribution [85]. The contact angle of liquid CaO–Al_2O_3–SiO_2–MgO inclusions in liquid steel is much smaller than 90° [72]. The negligible effect of melting rates on these

inclusions removal is expected to originate from such low contact angle which deteriorates the removal tendency of oxide inclusions from liquid steel in electroslag rapid remelting process.

4.4 Electrical parameters of ESR

In addition to the factors discussed in Sects. 4.1–4.3, the power supply (alternating current, direct current, and frequency) could also play a role in the removal and evolution of non-metallic inclusions in the ESR to some extent. During laboratory-scale ESR of Fe–Ni alloy and plain carbon steel, the dissolved aluminum and oxygen contents in liquid metal continuously increase due to inevitable electrochemical reactions in the ESR with a DC power supply, consequently giving rise to alumina inclusions formation in the liquid metal pool [129]. The increase in both total oxygen content and inclusion amount is more pronounced in Fe–Ni ingot. An increase in the amount of oxide inclusions in the hot work tool steel after ESR with lower frequency AC power supply, DC of reversed polarity, and DC of straight polarity was also reported by Paar et al. [130] on laboratory-scale experimental work. It should be stressed that these variations are different depending on the electrode material and the slag chemistry.

Different frequencies (2.5, 5.0, 7.5 and 50 Hz) of AC power supply of the laboratory-scale ESR experimentally proved that lower frequency AC power supply gave rise to a larger amount of inclusions in the remelted ingots because electrolytic reactions occur probably in the slag bath and the oxygen produced by electrolyzing in the slag bath enters the liquid metal pool [131]. Note that the chemical compositions and types of inclusions are not described in Ref. [131]. The laboratory-scale ESR with low frequencies of alternating current (1, 3 and 4.5 Hz) trials shows a similar finding, in which $MgO{\cdot}Al_2O_3$ and large calcium aluminates are oxide inclusion type in the H11 tool steel electrode [132]. Figure 14 presents a comparison of the content of different types of inclusions and the changes in oxygen content. The remelting at the frequency of 1 Hz leads not only to a significant increase in oxygen content, but also to a significant increase in oxide inclusion amount, both of which are much higher than that in the electrode. Increasing the frequency to 4.5 Hz leads to a reduction of total inclusions, which correlates to the slightly reduced oxygen content. The amount of oxide inclusions is much lower than that at lower frequencies but higher than that in the electrode. The larger amount of oxide inclusions is attributed to the electrolytic absorption of oxygen at lower frequency of ESR. It is evident that the composition of oxide inclusions changes towards higher Al_2O_3 content in the ESR with the frequency of 1 Hz, whereas the inclusion composition shifts towards a higher MgO content (spinel

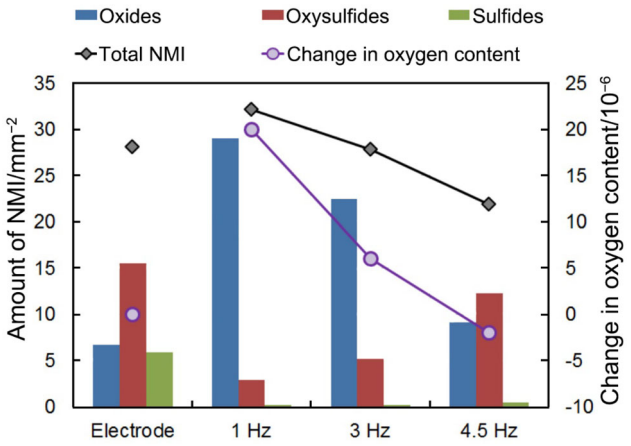

Fig. 14 Amount of non-metallic inclusions and oxygen content in ingots produced by ESR with different power supply frequencies [132]

type) and CaO rich oxides at higher frequency [132]. It could be due to the reaction between soluble aluminum and the increased soluble oxygen in liquid steel contributed by electrolytic absorption of oxygen.

Electroslag remelting production practices are widely operated with high frequency (50 or 60 Hz) of alternating current around the world. Regarding the role of power supply (alternating current, direct current, and frequency) on the steel cleanliness with respect to deoxidation and inclusions, the existing references are extremely limited. Despite these recent advances in low frequency ESR, there are still issues that will require more research in the future.

5 Effect of reoxidation of liquid steel during ESR on oxide inclusions

The introduction of oxygen from the ambient air and slag could hardly be avoided during ESR. Reoxidation of liquid steel by ambient air and slag has to be prevented for high-quality steel production. The details of oxygen transfer in the ESR process have been discussed by Shi et al. [133, 134]. Unlike the reoxidation of the liquid steel in other steelmaking process operations, in which the reoxidation may occur by several reasons, such as air exposure from open eyes in the ladle and tundish [135–137] and reaction with refractories [138], the reoxidation of liquid steel during ESR is dependent in a large part on the oxygen potential of the slag [32], besides the dissociation of original oxide inclusions [83] and the decomposition of components from slag [139], as well as permeation of atmospheric oxygen directly through molten slag into liquid metal pool by diffusion of physically dissolved oxygen which has been confirmed to play a minor role in soluble oxygen pickup [140–142]. The oxygen potential of the

ESR-type slag is typically determined by the iron oxide activity of the slag (in some cases, MnO is present in the slag, but in a quite small fraction).

The reoxidation of liquid steel always takes place during ESR of low-oxygen steel because of a big difference in the oxygen potential between liquid steel and the slag phase, as well as gas phase, even if protective inert atmosphere is employed throughout the ESR process [77, 85]. Reoxidation of liquid steel is a major problem in generating oxide inclusions [116, 143–145]. Reoxidation also results in consumption of alloying elements such as Al, Mn and Si in liquid steel, leading to oxide inclusion formation [146]. The reoxidation of liquid steel during ESR leads to considerable soluble oxygen pickup, which provides a driving force for the generation of fresh oxide inclusions. Some of the reoxidation results indeed show that the amount of oxide inclusions did not decrease after ESR, but increased [116]. For ESR of the steel electrode with 0.0018 mass% oxygen and CaO–Al_2O_3–SiO_2–MgO inclusions as the only oxide inclusions, it has been demonstrated that fresh CaO–Al_2O_3–MgO, MgO·Al_2O_3, and CaO–Al_2O_3–SiO_2–MgO inclusions are generated originating from the reactions taking place inside liquid steel in the liquid metal pool caused by reoxidation of liquid steel during the ESR, and these oxide inclusions are predominant inclusions in the remelted ingots [77]. The results from laboratory-scale open air atmosphere ESR trials show that the oxygen content of hot work tool steel almost doubled to 0.0024 mass%, leading to the formation of a large amount of new Al_2O_3 inclusions [116].

In addition to generation of fresh inclusions by reoxidation, the reoxidation of liquid steel during ESR could contribute to modification of the original oxide inclusion chemistry (resulting in their full liquefaction) and the increase in its size. The soluble oxygen supplied from the reoxidation of liquid steel and concerned elements in liquid steel react with the original semiliquid CaO–Al_2O_3–MgO inclusions that had not been removed in ESR process. With the progress of the transformation reaction, the MgO content of the oxide inclusion is diluted continuously, and consequently full liquid CaO–Al_2O_3–MgO–SiO_2 inclusions with a larger size are generated in industrial-scale ingots [85]. The reoxidation of liquid steel during conventional ESR and protective inert atmosphere ESR has become a normal phenomenon for low and ultra-low oxygen steel production. Reoxidation of liquid steel during protective argon gas atmosphere ESR that gives rise to generation of new oxide inclusions and modification of CaO–Al_2O_3–MgO inclusions has been confirmed in Ref. [77, 85]. More work is still needed to clarify the role of the reoxidation of liquid steel during ESR on the inclusions possessing different compositions and sizes together with its association with the compositions of steel and slag, as well as reveal its mechanism according to thermodynamics and kinetics.

6 Newly formed inclusions in remelted ingot

Fresh oxide inclusions could form at different stages of ESR, but fresh sulfide and nitride inclusions are generally generated during cooling and solidification of liquid metal in ESR. The newly formed oxide inclusions could be the products of the reaction between liquid steel and original inclusions from the electrode. In this section, the newly formed oxide inclusions originated from this route will not be discussed.

The compositions of the fresh oxide inclusions formed in liquid steel during ESR are dependent on the activity levels of oxygen and other species and the reaction kinetic condition [147]. Previous studies show that remelted ingot has same types of fresh inclusions as those in the liquid metal pool [77, 83], which is an indication of the absence of the formation of new types of inclusions even if fresh inclusions are formed during liquid steel solidification. No inclusions, which are relics from the electrode, were found in the liquid metal pool during pilot-scale protective argon atmosphere ESR [83]. Al_2O_3 and MgO·Al_2O_3 inclusions are formed in the liquid metal pool as a result of the reactions between alloying elements and the dissolved oxygen dissociated from MnO–SiO_2–Al_2O_3 inclusions in liquid steel. This experimental observation of oxide inclusions in the liquid metal pool is supported by thermodynamic calculation with FactSage (see Fig. 15) [83]. MgO·Al_2O_3 spinels and Al_2O_3 inclusions readily form in liquid steel at the temperatures much higher than the liquidus temperature of the steel as shown in Fig. 15.

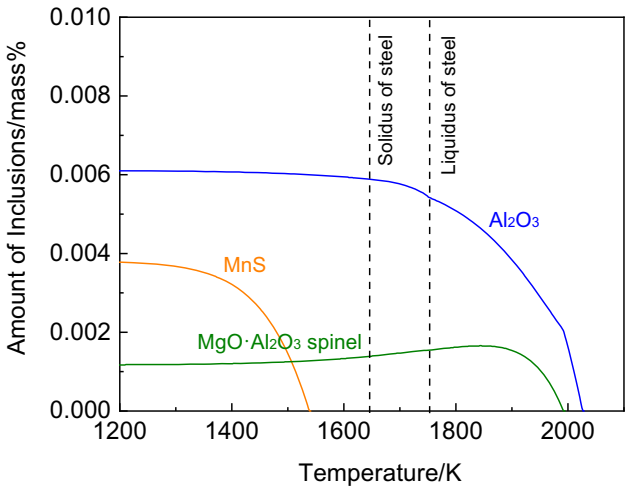

Fig. 15 Inclusions formation in steel as a function of temperature calculated with FactSage 7.2 [83]

$MgO{\cdot}Al_2O_3$ spinels and Al_2O_3 inclusions formed during cooling and solidification of liquid steel take up only a very small proportion of total oxide inclusions in remelted ingot. This proportion is mainly dependent on the activities of soluble oxygen and other inclusion-forming elements in liquid steel.

Fresh oxide inclusions would form since the soluble oxygen is supplied into liquid steel. This soluble oxygen could originate from not only the dissociation of original oxide inclusions into liquid steel, but also the reoxidation of liquid steel. Recent work in Refs. [77, 88] has confirmed the generation of new oxide inclusions in liquid metal pool caused by reoxidation of liquid steel during ESR. It has been noted in Refs. [77, 88] that the newly formed Al_2O_3 and $MgO{\cdot}Al_2O_3$ inclusions observed in liquid metal pool are spherical in their morphology. Al_2O_3 and $MgO{\cdot}Al_2O_3$ inclusions with spherical morphology form at high supersaturation of [O] and [Al] [148–150]. It suggests that the dissociation of original oxide inclusions and reoxidation of liquid steel during ESR give rise to a high soluble oxygen level of liquid steel.

In parallel, as a result of the reoxidation of liquid metal during ESR, two types of fresh oxide inclusions formed during ESR of Fe–25Ni–15Cr alloy in both liquid metal pool and laboratory-scale ingot, i.e., $MgO{\cdot}Al_2O_3$ spinels and complex inclusion of $MgO{\cdot}Al_2O_3$ spinel with an outer Ti_2O_3-rich layer [89]. The element mappings of typical inclusions observed in the liquid metal pool are illustrated in Fig. 16. $MgO{\cdot}Al_2O_3$ inclusions precipitate in the liquid metal pool during the ESR process according to Eq. (4).

$$2[Al] + [Mg] + 4[O] = (MgO{\cdot}Al_2O_3)_{inclusion} \quad (4)$$

As for the generation of $MgO{\cdot}Al_2O_3$ inclusions with an outer Ti_2O_3-rich layer, it is the reaction between soluble titanium in liquid alloy and $MgO{\cdot}Al_2O_3$ inclusion that forms an outer Ti_2O_3-rich layer on unreacted $MgO{\cdot}Al_2O_3$ inclusion core [89].

During industrial-scale protective argon gas atmosphere ESR of the bearing steel G20CrNi2Mo with low oxygen content (0.0012 mass%), reoxidation of liquid steel and oxide inclusion removal bring about an increase in the oxygen content up to 0.0020 mass% in the remelted ingot [26]. During this ESR process, all original oxide inclusions have been removed, as discussed in Sect. 3.1.2. Al_2O_3 inclusions smaller than 2 μm are generated at the slag/metal interface of electrode tip according to steel–slag reaction as expressed in Eq. (5) [26]

$$2[Al]+3(FeO)=(Al_2O_3)+3[Fe] \quad (5)$$

The thermodynamic calculation with FactSage 7.0 indicates that low-MgO $MgO–Al_2O_3$, Al_2O_3-based $CaO–Al_2O_3$(–MgO) and $CaO–Al_2O_3$ inclusions form in liquid steel during the ESR, which has been supported by the experimentally observed inclusions in remelted ingot [26]. It could be reasonably assumed that the reoxidation of liquid steel during ESR has contributed to the modification of oxide inclusion composition.

The liquid metal droplets pass through the molten slag pool and reach the liquid metal pool. The liquid metal solidifies directionally at the bottom of liquid metal pool and then builds as-cast ingot in a water-cooled mold. During cooling and solidification of liquid steel, the concentrations of non-metallic inclusion-forming elements gradually approach to saturation for inclusion formation. Fresh non-metallic inclusions would form once the oversaturation of these elements is reached at solidification front at the bottom of liquid metal pool. The source of inclusions in the remelted ingot formed in this way has been demonstrated for Al_2O_3 [55, 83, 116], $MgO{\cdot}Al_2O_3$ [83], AlN [87, 88], MnS [86], (Mn,Cr)S [25], and TiN [88–90, 109].

Even if fresh inclusion removal by floating up in liquid metal pool is possible, the removal in this pathway brings only an inappreciable contribution to overall inclusion removal, and elimination of the inclusions formed during

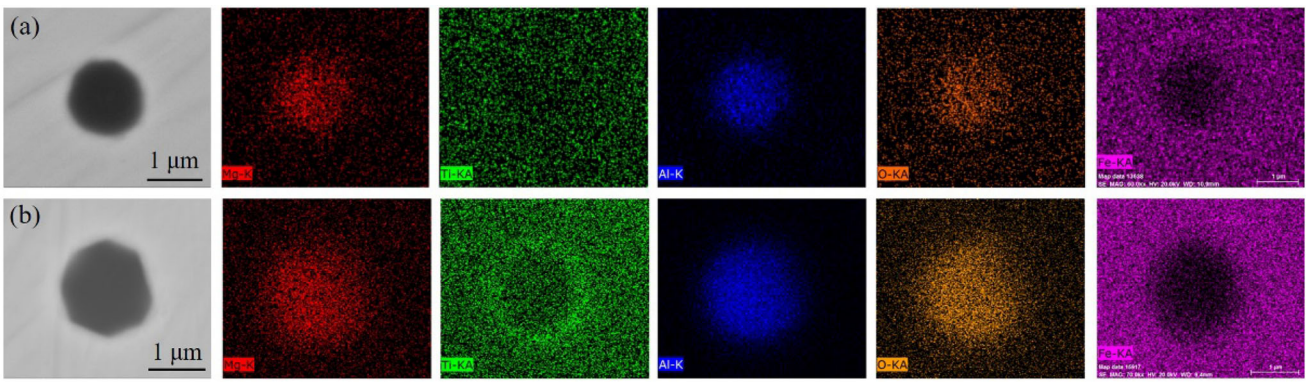

Fig. 16 SEM–EDS element mappings of typical inclusions observed in sample sampled from liquid metal pool during ESR. **a** $MgO{\cdot}Al_2O_3$ inclusion; **b** $MgO{\cdot}Al_2O_3$ inclusion with an outer $MgO–Al_2O_3–Ti_2O_3$ layer [89]

solidification of liquid steel in the ESR is almost impossible [36, 40, 41]. In most cases, these fresh inclusions significantly differ from the original inclusions in the electrode with regard to composition and size. These newly formed inclusions usually have small size.

Fu et al. [36, 151], Kay and Pomfret [40], and Mitchell [41] claimed that most even almost all of the inclusions in remelted ingot are the newly formed inclusions during the solidification of liquid steel in water-cooled mold. However, this is not always the case. Persson and Mitchell [15] reported that 50% of the inclusions in pilot-scale remelted ingot are relics from the electrode without a change in the ESR process. In the pilot-scale ESR of H13 steel electrodes deliberately containing a high content of several-millimeter-sized large oxide inclusions, only about 13.66% of these inclusions were removed during the ESR [16]. The sources of the inclusions in remelted ingot are summarized in Sect. 7. It is still a challenge to distinguish the fresh inclusions from the inclusions observed in remelted ingots.

7 Illustration of inclusion removal and fresh inclusion generation during ESR

In this section, the oxide inclusion removal and fresh inclusion generation during the ESR process are summarized. Non-metallic inclusions in liquid steel are removed during the ESR process in two ways (one or both work for a certain ESR case), i.e., (1) absorbing them into molten slag and (2) being dissociated in their individual chemical species into liquid steel. Inclusion removal into molten slag involves three steps: (i) transport to the steel/slag interface, (ii) separation into the slag phase across the slag/steel interface, (iii) dissolution in the slag. Inclusion removal into molten slag phase is the ultimate strategy for inclusion control of ESR. Among these three stages, step (i) is the rate-limiting step for oxide inclusion removal during ESR [18].

Inclusion removal takes place at three process stages of ESR, which do, more or less, contribute to the overall inclusion removal. In the liquid metal film formation and its collection into droplet process at the electrode tip (stage I), many of the original oxide inclusions are rejected to the slag/liquid metal interface. Most if not all of these oxide inclusions exposed to the steel/slag interface would separate into slag and substantially dissolve in molten slag. The original oxide inclusions that have not been removed at stage I remain in the metal droplets falling from the electrode. The other two stages are that movement of the metal droplets passing through the molten slag pool (stage II) and gathering of liquid metal in liquid metal pool (stage III). It is suggested that inclusion removal by flotation up in liquid metal pool is possible, but does not play an important role with regard to the removal of non-metallic inclusions in ESR.

The inclusion removal and fresh inclusion generation during the ESR process are schematically summarized in Fig. 17. For some kinds of oxide and sulfide inclusions, dissolution of the inclusions in its individual chemical species into liquid steel would occur. Inclusion removal in this trajectory is completed before the liquid metal droplets collect in the liquid metal pool [21, 25, 47, 55, 67, 83, 85].

Fresh oxide inclusions could be generated by the reactions taking place inside liquid steel as reoxidation products at stages I, II and III (see Fig. 17). Fresh oxide inclusions could also be products of the reactions between the soluble oxygen that arise from the dissociation of original oxide inclusions and other dissolved species in liquid steel [O] + [M] = (MO). Furthermore, stage IV, precipitation of new non-metallic inclusions during cooling and solidification of liquid steel in ESR is another source.

The behavior of TiN, low-melting-temperature CaO–Al_2O_3–SiO_2–MgO, and MnO–SiO_2–Al_2O_3 inclusions on the surface of liquid steel has been studied with in situ confocal laser scanning microscopy [84, 152, 153], so as to identify possible physical mechanisms of these inclusions removal based on in situ disappearance of these inclusions on the surface of liquid steel. Combining with this physical mechanism, more study is needed to clarify these types of inclusions removal in the ESR process and examine its thermodynamic and kinetic mechanisms in terms of steel composition.

The non-metallic inclusions in the remelted ingot would originate from one or more of the following routes: (1) the original inclusions that have not been removed in the ESR process, (2) steel–original inclusion reaction products (for many cases [85], the original inclusions that have not been removed in the ESR process would experince composition change caused by steel–inclusion reaction in the ESR), (3) reaction products of alloying elements and the dissolved oxygen dissociated from original oxide inclusions and/or caused by reoxidation [83], (4) the inclusions newly formed during cooling and solidification of liquid steel in the ESR [83].

8 Concluding remarks

Non-metallic inclusions with different compositions and sizes from the electrode basically experience various evolution trajectories during the ESR, including absorption by slag, composition modification by steel–inclusion reaction, and/or dissociation in its individual chemical species into liquid steel. The evolution of these inclusions is also dependent on one or more of other processing parameters, including liquid metal composition, slag chemistry,

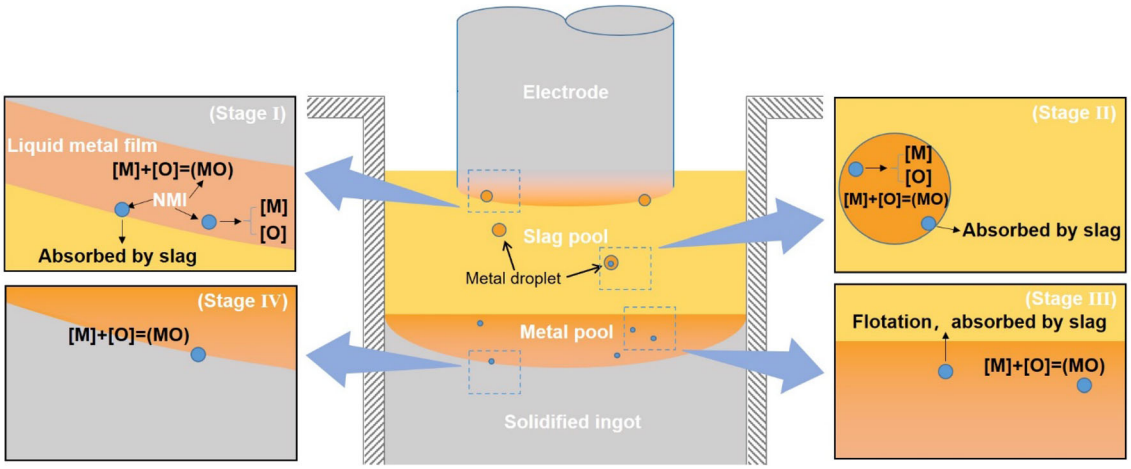

Fig. 17 Schematic illustration of inclusion removal and fresh inclusion generation during ESR process

deoxidation scheme, melting rate, electrical parameters, etc. These evolution trajectories determine the removal efficiency of inclusions in the ESR, and the composition and size of inclusions (the relics from the electrode, modified composition of original inclusions or newly formed inclusions) in remelted ingot. Deoxidation of ESR is quietly needed because of its significant contribution to reduction of inclusion amount, retardation of new inclusion formation and modification of oxide inclusion composition. Melting rates of ESR have only a limited effect on inclusion removal. Nevertheless, more research is needed to assess the effect of melting rate on the modification of oxide inclusion composition, as well as the formation and removal of new inclusions.

Generation of new inclusions during ESR is inevitable. Fresh oxide inclusions could form at different stages of ESR, but fresh sulfide and nitride inclusions are generally generated during cooling and solidification of liquid metal in ESR. The contribution of oxide inclusions formed at the different stages to the overall oxide inclusions in remelted ingot is dependent on the activities of species in liquid steel at different timescales. More attentions have to be paid to the reoxidation of liquid steel during the ESR. It is inevitable during the ESR of low oxygen steel, even if protective inert atmosphere is employed throughout the ESR process. The reoxidation during the ESR results in not only an increase in the amount of inclusions caused by new oxide inclusion formation, but also modification of oxide inclusion composition. More work is still needed to ascertain the role of the reoxidation of liquid steel during ESR on the inclusions possessing different compositions and sizes together with its association with the compositions of steel and slag.

Acknowledgements The financial support by the National Natural Science Foundation of China (Grant Nos. 51874026 and 52074027) and the Fundamental Research Funds for the Central Universities (Grant No. FRF-AT-20-13) is greatly acknowledged. The authors are also thankful to the financial support from the State Key Laboratory of Advanced Metallurgy (Grant No. 41621024).

References

[1] J.H. Park, H. Todoroki, ISIJ Int. 50 (2010) 1333–1346.
[2] Y. Murakami, M. Endo, Int. J. Fatigue 16 (1994) 163–182.
[3] F. Meurling, A. Melander, M. Tidesten, L. Westin, Int. J. Fatigue 23 (2001) 215–224.
[4] W.M. Garrison, A.L. Wojcieszynski, Mater. Sci. Eng. A. 464 (2007) 321–329.
[5] P.A. Thornton, J. Mater. Sci. 6 (1971) 347–356.
[6] Y. Tomita, Mater. Charact. 34 (1995) 121–128.
[7] I.I. Reformatskaya, I.G. Rodionova, Y.A. Beilin, L.A. Nisel'son, A.N. Podobaev, Prot. Met. 40 (2004) 447–452.
[8] T.V. Shibaeva, V.K. Laurinavichyute, G.A. Tsirlina, A.M. Arsenkin, K.V. Grigorovich, Corros. Sci. 80 (2014) 299–308.
[9] S.K. Dhua, A. Ray, S.K. Sen, M.S. Prasad, K.B. Mishra, S. Jha, J. Mater. Eng. Perform. 9 (2000) 700–709.
[10] J. Zhou, D.S. Ma, C.M. Zhang, A.J. Kang, X.Y. Li, Z.Z. Chen, Heat Treat. Met. 37 (2012) 53–58.
[11] Y.B. Zhong, L. Qiang, Y.P. Fang, H. Wang, M.H. Peng, L.C. Dong, T.X. Zheng, Z.S. Lei, W.L. Ren, Z.M. Ren, Mater. Sci. Eng. A. 660 (2016) 118–126.
[12] M. Schwenk, B. Friedrich, in: Proc. Liquid Metal Processing and Casting Conf. 2017, The Minerals, Metals & Materials Society, Pittsburgh, PA, USA, 2017, pp. 225–229.
[13] Q.T. Zhu, J. Li, J. Zhang, C.B. Shi, J.H. Li, J. Huang, Metall. Mater. Trans. B 50 (2019) 1365–1377.
[14] S.F. Yang, S.L. Yang, J.L. Qu, J.H. Du, Y. Gu, P. Zhao, N. Wang, J. Iron Steel Res. Int. 28 (2021) 921–937.
[15] E.S. Persson, A. Mitchell, in: Proc. Liquid Metal Processing and Casting Conf. 2017, The Minerals, Metals & Materials Society, Pittsburgh, PA, USA, 2017, pp. 373–379.
[16] G. Du, J. Li, Z.B. Wang, Ironmak. Steelmak. 45 (2018) 919–923.

[17] A. Choudh, ISIJ Int. 32 (1992) 563–574.
[18] Z.B. Li, J.W. Zhang, X.Q. Che, J. Iron Steel Res. 9 (1997) 7–12.
[19] A. Paar, R. Schneider, P. Zeller, G. Reiter, S. Paul, I. Silier, P. Würzinger, in: Proc. Liquid Metal Processing and Casting Conf. 2013, The Minerals, Metals & Materials Society, Austin, USA, 2013, pp. 29–36.
[20] B. Podgornik, V. Leskovšek, M. Godec, B. Senčič, Mater. Sci. Eng. A 599 (2014) 81–86.
[21] E.S. Persson, A. Karasev, P. Jönsson, in: Liquid Metal Processing and Casting Conf. 2017, The Minerals, Metals & Materials Society, Pittsburgh, PA, USA, 2017, pp. 353–360.
[22] M. Chatterjee, M.S.N. Balasubramanian, K.M. Gupt, P.K. Rao, Ironmak. Steelmak. 17 (1990) 38–42.
[23] C.B. Shi, X.C. Chen, F. Wang, H.J. Guo, in: Materials Science & Technology 2012 Conf. and Exhibition Proc., The Minerals, Metals and Materials Society, Warrendale, PA, USA, 2012, pp. 1261–1268.
[24] S. Radwitz, H. Scholz, B. Friedrich, H. Franz, in: International Symposium on Liquid Metal Processing & Casting 2015, Leoben, Austria, 2015, pp. 153–162.
[25] Y. Liu, Z. Zhang, G.Q. Li, Q. Wang, L. Wang, B.K. Li, Steel Res. Int. 88 (2017) 1700058.
[26] S.J. Li, G.G. Cheng, Z.Q. Miao, W.X. Dai, L. Chen, Z.Q. Liu, ISIJ Int. 58 (2018) 1781–1790.
[27] T. Uesugi, Tetsu-to-Hagané 74 (1988) 1889–1894.
[28] D.G. Zhou, X.C. Chen, J. Fu, P. Wang, J. Li, M.D. Xu, J. Univ. Sci. Technol. Beijing, 22 (2000) 26–30.
[29] D.G. Zhou, J. Fu, X.C. Chen, J. Li, J. Univ. Sci. Technol. Beijing 8 (2001) 25–27.
[30] J.G. Yang, J.H. Park, Metall. Mater. Trans. B 48 (2017) 2147–2156.
[31] D. Hou, Z. Jiang, Y. Dong, W. Gong, Y. Cao, H. Cao, ISIJ Int. 57 (2017) 1400–1409.
[32] C.B. Shi, ISIJ Int. 60 (2020) 1083–1096.
[33] C.B. Shi, Y. Huang, J.X. Zhang, J. Li, X. Zheng, Int. J. Miner. Metall. Mater. 28 (2021) 18–29.
[34] M.M. Klyuyev, F.F. Tonilin, Journal of Ferrous Metallurgy 1 (1962) 78–80.
[35] O. Madono, Production of aluminum-iron base alloys by electroslag melting, in: Proceedings of the Second International Symposium on Electroslag Remelting Technology, Pittsburgh, USA, 1969.
[36] J. Fu, J. Zhu, Acta Metall. Sin. 7 (1964) 250–262.
[37] Z.B. Li, Y.D. Li, Y.W. Ye, Z.C. Song, Iron and Steel (1966) No. 1, 20–24.
[38] Z.B. Li, W.H. Zhou, Y.D. Li, Iron and Steel 15 (1980) 20–26.
[39] P.P. Evseyev, A.F. Filippov, Izvest. Akad. Nauk SSSR, Metally 3 (1968) 41–43.
[40] D.A.R. Kay, R.J. Pomfret, J. Iron Steel Inst. 209 (1971) 962–965.
[41] A. Mitchell, Ironmak. Steelmak. 1 (1974) 172–179.
[42] R.G. Baligidad, U. Prakash, V.R. Rao, P.K. Rao, N.B. Ballal, Ironmak. Steelmak. 21 (1994) 324–331.
[43] S.K. Jo, B. Song, S.H. Kim, Metall. Mater. Trans. B 33 (2002) 703–709.
[44] W.G. Seo, W.H. Han, J.S. Kim, J.J. Pak, ISIJ Int. 43 (2003) 201–208.
[45] H. Todoroki, K. Mizuno, Iron Steelmaker 30 (2003) 60–67.
[46] E.B. Pretorius, H.G. Oltmann, T. Cash, Iron Steel Technol. 7 (2010) 31–44.
[47] C.B. Shi, W.T. Yu, H. Wang, J. Li, M. Jiang, Metall. Mater. Trans. B 48 (2017) 146–161.
[48] M.K. El-Fawkhry, A.M. Fathy, M.M. Eissa, Steel Res. Int. 85 (2014) 885–890.
[49] J. Li, J. Li, C.B. Shi, L.L. Wang, Z. Wu, H. Wang, Can. Metall. Quart. 55 (2016) 321–327.
[50] P.N. Quested, M. Mclean, Mater. Sci. Eng. 65 (1984) 171–180.
[51] N. Verma, P.C. Pistorius, R.J. Fruehan, M.S. Potter, H.G. Oltmann, E.B. Pretorius, Metall. Mater. Trans. B 43 (2012) 830–840.
[52] H. Suito, R. Inoue, ISIJ Int. 36 (1996) 528–536.
[53] M.A.T. Andersson, P.G. Jönsson, M.M. Nzotta, ISIJ Int. 39 (1999) 1140–1149.
[54] C. Wagner, Thermodynamics of alloys, Addison-Wesley Press, Cambridge, UK, 1952.
[55] C.B. Shi, X.C. Chen, H.J. Guo, Z.J. Zhu, H. Ren, Steel Res. Int. 83 (2012) 472–486.
[56] X.Y. Gao, L. Zhang, X.H. Qu, Y.F. Luan, X.W. Chen, Metall. Res. Technol. 117 (2020) 501–509.
[57] E.S. Persson, A. Karasev, A. Mitchell, P.G. Jönsson, Metals 10 (2020) 1620–1635.
[58] X.C. Chen, C.B. Shi, H.J. Guo, F. Wang, H. Ren, D. Feng, Metall. Mater. Trans. B 43 (2012) 1596–1607.
[59] L. Holappa, M. Hämäläinen, M. Liukkonen, M. Lind, Ironmak. Steelmak. 30 (2003) 111–115.
[60] S.R. Story, R.I. Asfahani, in: AISTech 2013 Proc., Vol. II, Association for Iron & Steel Technology, Pittsburgh, PA, USA, 2013, pp. 1201–1213.
[61] Y.I. Ito, S. Nara, Y. Kato, M. Suda, Tetsu-to-Hagané 93 (2007) 355–361.
[62] Z. Deng, M. Zhu, Steel Res. Int. 84 (2013) 519–525.
[63] M. Lind, L. Holappa, Metall. Mater. Trans. B 41 (2010) 359–366.
[64] J.H. Park, D.S. Kim, S.B. Lee, Metall. Mater. Trans. B 36 (2005) 67–73.
[65] N. Verma, P.C. Pistorius, R.J. Fruehan, M. Potter, M. Lind, S.R. Story, Metall. Mater. Trans. B 42 (2011) 711–719.
[66] N. Verma, P.C. Pistorius, R.J. Fruehan, M. Potter, M. Lind, S.R. Story, Metall. Mater. Trans. B 42 (2011) 720–729.
[67] C.B. Shi, X.C. Chen, H.J. Guo, Z.J. Zhu, X. Sun, Metall. Mater. Trans. B 44 (2013) 378–389.
[68] G.W. Yang, X.H. Wang, F.X. Huang, D. Yang, P.Y. Wei, X. Hao, Metall. Mater. Trans. B 46 (2015) 145–154.
[69] A.L. Kundu, K.M. Gupt, P.K. Rao, Metall. Mater. Trans. B 20 (1989) 581–594.
[70] J. Wikström, K. Nakajima, H. Shibata, A. Tilliander, P. Jönsson, Mater. Sci. Eng. A 495 (2008) 316–319.
[71] B.H. Reis, W.V. Bielefeldt, A.C.F. Vilela, ISIJ Int. 54 (2014) 1584–1591.
[72] T. Yoshioka, K. Nakahata, T. Kawamura, Y. Ohba, ISIJ Int. 56 (2016) 1973–1981.
[73] X. Zheng, P.C. Hayes, H.G. Lee, ISIJ Int. 37 (1997) 1091–1097.
[74] J.S. Cho, H.G. Lee, ISIJ Int. 41 (2001) 151–157.
[75] H. Arai, K. Matsumoto, S. Shimasaki, S. Taniguchi, ISIJ Int. 49 (2009) 965–974.
[76] T. Yoshioka, T. Ideguchi, A. Karasev, Y. Ohba, P.G. Jönsson, Steel Res. Int. 89 (2017) 1700287.
[77] C.B. Shi, H. Wang, J. Li, Metall. Mater. Trans. B 49 (2018) 1675–1689.
[78] H. Wang, C.M. Shi, J. Li, C.B. Shi, Y.F. Qi, Ironmak. Steelmak. 45 (2018) 6–16.
[79] Y.W. Dong, Z. Jiang, Y. Cao, A. Yu, D. Hou, Metall. Mater. Trans. B 45 (2014) 1315–1324.
[80] K. Wang, M. Jiang, X. Wang, Y. Wang, H. Zhao, Z. Cao, Metall. Mater. Trans. B 46 (2015) 2198–2207.
[81] A. García-Carbajal, M. Herrera-Trejo, E.I. Castro-Cedeño, M. Castro-Román, A.I. Martinez-Enriquez, Metall. Mater. Trans. B 48 (2017) 3364–3379.

[82] J.S. Park, J.H. Park, Metall. Mater. Trans. B 45 (2014) 953–960.
[83] C.B. Shi, J.H. Park, Metall. Mater. Trans. B 50 (2019) 1139–1147.
[84] W.J. Liu, J. Li, H. Wang, C.B. Shi, Steel Res. Int. 90 (2019) 1900185.
[85] C.B. Shi, D.L. Zheng, B.S. Guo, J. Li, F. Jiang, Metall. Mater. Trans. B 49 (2018) 3390–3402.
[86] Y.F. Qi, J. Li, C.B. Shi, H. Wang, D.L. Zheng, Metall. Res. Technol. 116 (2019) 322–333.
[87] C.B. Shi, X.C. Chen, H.J. Guo, Int. J. Miner. Metall. Mater. 19 (2012) 295–302.
[88] X. Huang, B. Li, Z. Liu, T. Jiang, Y. Chai, X. Wu, Vacuum 164 (2019) 114–120.
[89] D.L. Zheng, J. Li, C.B. Shi, J. Zhang, R.M. Geng, ISIJ Int. 60 (2020) 1577–1585.
[90] H.J. Miao, Y. Wang, L. Zeng, Y. Li, Iron and Steel 48 (2013) No. 6, 67–69.
[91] J.D. Busch, J.J. Debarbadillo, M.J.M. Krane, Metall. Mater. Trans. A 44 (2013) 5295–5303.
[92] F. Reyes-Carmona, A. Mitchell, ISIJ Int. 32 (1992) 529–537.
[93] A. Mitchell, F. Reyes-Carmona, E. Samuelsson, Trans. Iron Steel Inst. Jpn. 24 (1984) 547–556.
[94] D.A.R. Kay, A. Mitchell, M. Ram, J. Iron Steel Inst. 208 (1970) 141–146.
[95] J. Wei, A. Mitchell, Acta Metall. Sin. 23 (1987) 126–134.
[96] J. Wei, Chin. J. Met. Sci. Technol. 5 (1989) 235–246.
[97] S. Li, G. Cheng, Z. Miao, L. Chen, X. Jiang, Int. J. Miner. Metall. Mater. 26 (2019) 291–300.
[98] A. Mitchell, F.R. Carmona, C. Wei, Iron Steelmaker 9 (1982) 37–41.
[99] D. Xiang, X. Zhu, K. Wang, J. Iron Steel Res. 1 (1989) 9–14.
[100] P. Wen, D. Xiang, Heavy Cast. Forg. 1 (2016) 23–25.
[101] A. Sekiya, S. Nakayama, T. Taketsuru, Denki-Seiko 66 (1995) 47–53.
[102] S.F. Yang, J.S. Li, L.F. Zhang, K.D. Peaslee, G. Li, in: AISTech 2012 Proc. Association for Iron & Steel Technology, Warrendale, PA, USA, 2012, pp. 47–55.
[103] C.B. Shi, X.C. Chen, H.J. Guo, in: AISTech 2012 Proc., Association for Iron & Steel Technology, Warrendale, PA, USA, 2012, pp. 947–957.
[104] S.F. Medina, A. Cores, ISIJ Int. 33 (1993) 1244–1251.
[105] G. Pateisky, H. Biele, H.J. Fleischer, J. Vac. Sci. Technol. 9 (1972) 1318–1322.
[106] M. Detrois, P.D. Jablonski, J.A. Hawk, Metall. Mater. Trans. B 50 (2019) 1686–1695.
[107] J.W. Zhang, Y. Xiong, Special Steel 19 (1998) 6–9.
[108] S. Radwitz, H. Scholz, B. Friedrich, H. Franz, in: Proc. European Metallurgical Conf. 2015, Vol. 2, GDMB Society of Metallurgists and Miners, Düsseldorf, 2015, pp. 887–896.
[109] J. Burja, F. Tehovnik, M. Godec, J. Medved, B. Podgornik, R. Barbič, J. Min. Metall. Sect. B-Metall. 54 (2018) 51–57.
[110] D. Hou, D.Y. Wang, Z.H. Jiang, T.P. Qu, H.H. Wang, J.W. Dong, Metall. Mater. Trans. B 52 (2021) 478–493.
[111] M. Allibert, J.F. Wadier, A. Mitchell, Ironmak. Steelmak. 5 (1978) 211–216.
[112] C.B. Shi, J. Li, J.W. Cho, F. Jiang, I. Jung, Metall. Mater. Trans. B 46 (2015) 2110–2120.
[113] D.S. Kim, G.J. Lee, M.B. Lee, J.I. Hur, J.W. Lee, in: International of Symposium on Liquid Metal Processing & Casting 2015, Leoben, Austria, 2015, pp. 43–52.
[114] Y.B. Kang, H.G. Lee: ISIJ Int. 44 (2004) 1006–1015.
[115] R. Schneider, C. Schüller, P. Würzinger, G. Reiter, C. Martinez, BHM Berg-und Hüttenmänn. Monatsh. 160 (2015) 117–122.
[116] R.S.E. Schneider, M. Molnar, S. Gelder, G. Reiter, C. Martinez, Steel Res. Int. 89 (2018) 1800161.
[117] R.S.E. Schneider, M. Molnar, G. Klösch, C. Schüller, J. Fasching, Steel Res. Int. 91 (2020) 2000241.
[118] R.S.E. Schneider, M. Molnar, G. Klösch, C. Schüller. J. Fasching. Metall. Mater. Trans. B 51 (2020) 1904–1911.
[119] T.J. Wen, Q. Ren, L.F. Zhang, J.J. Wang, Y. Ren, J. Zhang, W. Yang, A.J. Xu, Steel Res. Int. 92 (2021) 2000629.
[120] D.G. Zhou, C.S. Wang, M. Qian, M.D. Xu, Z.B. Li, J.W. Zhang, Iron and Steel 29 (1994) No. 7, 25–28.
[121] S.X. Yang, H.B. Li, H. Feng, Z.H. Jiang, M. Chen, T. He, Metall. Mater. Trans. B. 52 (2021) 1294–1308.
[122] W. Holzgruber, K. Petersen, P.E. Schneider, in: Transaction of the International Vacuum Metallurgy Conference, California, US, 1968, pp. 499–523.
[123] M.E. Fraser, A. Mitchell, Ironmak. Steelmak. 3 (1976) 279–287.
[124] B. Hernandez-Morales, A. Mitchell, Ironmak. Steelmak. 26 (1999) 423–438.
[125] L. Rao, J.H. Zhao, Z.X. Zhao, G. Ding, M.P. Geng, J. Iron Steel Res. Int. 21 (2014) 644–652.
[126] S. Ahmadi, H. Arabi, A. Shokuhfar, A. Rezaei, J. Mater. Sci. Technol. 25 (2009) 592–596.
[127] C.B. Shi, X. Zheng, Z.B. Yang, P. Lan, J. Li, F. Jiang, Met. Mater. Int. 27 (2021) 3603–3616.
[128] J.C. Korp, M. Kubin, in: INTECO Remelting & Forging Symposium Shanghai 2010 – Proceedings, Shanghai, China, 2010, pp. 73–88.
[129] M. Kawakami, T. Takenaka, M. Ishikawa, Ironmak. Steelmak. 29 (2002) 287–292.
[130] A. Paar, R. Schneider, P. Zeller, G. Reiter, S. Paul, P. Würzinger, Steel Res. Int. 85 (2014) 570–578.
[131] L.Z. Chang, X.F. Shi, H.S. Yang, Z.B. Li, J. Iron Steel Res. Int. 16 (2009) No. 4, 7–11.
[132] R. Schneider, M. Mülleder, P. Zeller, P. Würzinger, G. Reiter, S. Paul, in: International of Symposium on Liquid Metal Processing & Casting 2015, Leoben, Austria, 2015, pp. 23–31.
[133] C.B. Shi, X.C. Chen, Y.W. Luo, H.J. Guo, in: Materials Processing Fundamentals, The Minerals, Metals and Materials Society, Warrendale, PA, 2013, pp. 31–38.
[134] C.B. Shi, Behaviour and control technique of oxygen and inclusions during protective atmosphere electroslag remelting process, University of Science and Technology Beijing, Beijing, China, 2012.
[135] P. Valentin, C. Bruch, Y. Kyrylenko, H. Köchner, C. Dannert, Steel Res. Int. 80 (2009) 552–558.
[136] M. Thunman, S. Eckert, O. Hennig, J. Björkvall, D. Sichen, Steel Res. Int. 78 (2007) 849–856.
[137] S. Chatterjee, D. Li, K. Chattopadhyay, Steel Res. Int. 88 (2017) 1600436.
[138] E. Zinngrebe, J. Small, S.V.D. Laan, A. Westendorp, Metall. Mater. Trans. B 51 (2020) 2321–2338.
[139] L.Z. Chang, X.F. Shi, J.Q. Cong, Ironmak. Steelmak. 41 (2014) 182–186.
[140] M. Sasabe, K.S. Goto, Metall. Trans. 5 (1974) 2225–2233.
[141] M. Sasabe, Y. Kinoshita, Tetsu-to-Hagané 65 (1979) 1727–1736.
[142] J.H. Wei, Z.Y. Liu, Acta Metall. Sin. 30 (1994) 350–360.
[143] D.C. Park, I.H. Jung, P.C.H. Rhee, H.G. Lee, ISIJ Int. 44 (2004) 1669–1678.
[144] W. Tiekink, R. Boom, A. Overbosch, R. Kooter, S. Sridhar, Ironmak. Steelmak. 37 (2010) 488–495.
[145] T.S. Kim, Y. Chung, L. Holappa, J.H. Park, Metall. Mater. Trans. B 48 (2017) 1736–1747.
[146] B. Coletti, B. Gommers, C. Vercruyssen, B. Blanpain, P. Wollants, F. Haers, Ironmak. Steelmak. 30 (2003) 101–105.

[147] E.Y. Kolpishon, M.V. Ivanova, S.Y. Afanas'ev, E.V. Shytov, Russian Metallurgy (Metally) 2007 (2007) 591–593.
[148] M.A.V. Ende, M.X. Guo, B. Blanpain, P. Wollants, Front. Mater. Sci. 5 (2011) 69–76.
[149] O. Adaba, R.J. O'malley, L.N. Bartlett, Metall. Mater. Trans. B 51 (2020) 1679–1686.
[150] R. Dekkers, B. Blanpain, P. Wollants, Metall. Mater. Trans. B 34 (2003) 161–171.
[151] D.G. Zhou, W.G. Xu, P. Wang, J. Fu, J.H. Xu, C.S. Wang, M.D. Xu, Iron and Steel 33 (1998) No. 3, 13–17.
[152] L. Yang, G.G. Cheng, S.J. Li, M. Zhao, G.P. Feng, ISIJ Int. 55 (2015) 1901–1905.
[153] H. Wang, J. Li, C.B. Shi, Y.F. Qi, Y.X. Dai, ISIJ Int. 59 (2019) 828–838.